The Plant Cell, Vol. 29: 3068–3084, December 2017, www.plantcell.org © 2017 ASPB.

Check for updates

Intracellular Distribution of Manganese by the *Trans*-Golgi Network Transporter NRAMP2 Is Critical for Photosynthesis and Cellular Redox Homeostasis

Santiago Alejandro,[a,1] Rémy Cailliatte,[a,1] Carine Alcon,[a] Léon Dirick,[a] Frédéric Domergue,[b] David Correia,[a] Loren Castaings,[a] Jean-François Briat,[a] Stéphane Mari,[a] and Catherine Curie[a,2]

[a] BPMP, CNRS, INRA, Montpellier SupAgro, Université de Montpellier, F-34060 Montpellier, France
[b] Laboratoire de Biogénèse Membranaire CNRS, Université de Bordeaux, UMR 5200, F-33140 Villenave d'Ornon, France

ORCID IDs: 0000-0002-0806-3378 (R.C.); 0000-0002-0183-7000 (F.D.); 0000-0002-8884-1175 (C.C.)

Plants require trace levels of manganese (Mn) for survival, as it is an essential cofactor in oxygen metabolism, especially O_2 production via photosynthesis and the disposal of superoxide radicals. These processes occur in specialized organelles, requiring membrane-bound intracellular transporters to partition Mn between cell compartments. We identified an *Arabidopsis thaliana* member of the NRAMP family of divalent metal transporters, NRAMP2, which functions in the intracellular distribution of Mn. Two knockdown alleles of *NRAMP2* showed decreased activity of photosystem II and increased oxidative stress under Mn-deficient conditions, yet total Mn content remained unchanged. At the subcellular level, these phenotypes were associated with a loss of Mn content in vacuoles and chloroplasts. NRAMP2 was able to rescue the mitochondrial yeast mutant *mtm1*Δ. In plants, NRAMP2 is a resident protein of the *trans*-Golgi network. NRAMP2 may act indirectly on downstream organelles by building up a cytosolic pool that is used to feed target compartments. Moreover, not only does the *nramp2* mutant accumulate superoxide ions, but NRAMP2 can functionally replace cytosolic superoxide dismutase in yeast, indicating that the pool of Mn displaced by NRAMP2 is required for the detoxification of reactive oxygen species.

INTRODUCTION

Mn serves as a cofactor for an array of enzymes and pathways, the most important of which is the antioxidant defense enzyme manganese superoxide dismutase (Mn SOD), which dismutates superoxide anion into the less toxic hydrogen peroxide and oxygen in mitochondria and peroxisomes (del Río et al., 2003). In addition, photosynthetic organisms use Mn in the reaction center of PSII, in which a four Mn-cluster coordinates with the oxygen evolving complex to perform the water-splitting reaction (Nickelsen and Rengstl, 2013). For these reasons, Mn deficiency in plants targets two essential cellular functions: antioxidant capacity and photosynthetic activity. Although Mn is rarely limiting for animal cells, its bioavailability to plants is dramatically reduced in dry, well-aerated, and alkaline soils, which negatively affects plant growth. Visual symptoms of Mn shortage are limited to young leaves, which are chlorotic at moderate deficiency but develop necrosis at extreme deficiency levels (Schmidt et al., 2016). Consequently, the agronomical repercussions of Mn deficiency have been underestimated and the molecular mechanisms at work in the response to Mn limitation have been little explored compared with those of other essential metals such as Fe, Zn, and Cu. Mn excess can also be detrimental to organisms. Mn toxicity leads to a predisposition to genomic instability (García-Rodríguez et al., 2012) and causes a neurological syndrome in human called manganism, with symptoms resembling those of Parkinson disease (Roth, 2006). In plants, Mn toxicity is widespread in acidic soils, where it becomes more available and provokes quite diverse symptoms often characterized by brown speckles containing oxidized Mn on mature leaves and/or interveinal chlorosis and necrosis (Marschner et al., 1986).

Most species acquire Mn via transporters of the natural resistance-associated macrophage protein (NRAMP) family. These divalent metal/proton symporters harbor a broad range specificity for metals (Nevo and Nelson, 2006). In *Arabidopsis thaliana* and rice (*Oryza sativa*), high-affinity Mn uptake in root depends on the presence of NRAMP1 and NRAMP5, respectively, at the root surface. Loss of function of Arabidopsis *NRAMP1* or rice *NRAMP5* dramatically decreases the tolerance of the plant to Mn deficiency (Cailliatte et al., 2010; Ishimaru et al., 2012; Sasaki et al., 2012). These proteins are therefore true orthologs of the NRAMP transporter Smf1p in yeast (Cohen et al., 2000). Moreover, in most species, Mn is a substrate of the high-affinity, root-surface-localized Fe uptake transporter IRT1, which was shown in Arabidopsis to contribute to Mn acquisition when combined with the *nramp1* mutation (Castaings et al., 2016).

Our understanding of the mechanisms of the intracellular distribution of Mn is still fragmentary. In plants, trafficking of Mn across the membranes of major organelles is mediated by transporters belonging to a variety of transporter families. In seeds, the tonoplastic VIT1 transporter mediates import of Mn and Fe into the vacuole (Kim et al., 2006; Momonoi et al., 2009; Zhang et al., 2012) from where these metals are remobilized in Arabidopsis by the NRAMP transporters NRAMP3 and NRAMP4. By mediating Mn efflux from the vacuole, these two highly homologous tonoplastic

[1] These authors contributed equally to this work.
[2] Address correspondence to catherine.curie@cnrs.fr.
The author responsible for distribution of materials integral to the findings presented in this article in accordance with the policy described in the Instructions for Authors (www.plantcell.org) is: Catherine Curie (catherine.curie@cnrs.fr).
www.plantcell.org/cgi/doi/10.1105/tpc.17.00578

proteins help maintain efficient PSII activity under Mn-limiting conditions (Lanquar et al., 2005, 2010). Mn vacuolar transporters also include (1) CAX2, a Ca^{2+}/cation antiporter involved in the vacuolar sequestration of Mn (Pittman et al., 2004); (2) ZIP1, a homolog of IRT1 located within the tonoplast membrane of root stele cells, where it is thought to participate in the remobilization of Mn from the vacuole to the cytosol and mediate radial movement of Mn in the root (Milner et al., 2013); and (3) METAL TOLERANT PROTEIN8 members in rice (Os-MTP8.1) and Arabidopsis (MTP8), which belong to the subgroup of cation diffusion facilitators (CDFs) involved in proton/Mn antiport that help protect the cell from Mn toxicity by targeting excess cytosolic Mn to the vacuole (Eroglu et al., 2016). How Mn is transported into mitochondria is currently unknown. A study in yeast (*Saccharomyces cerevisiae*) initially identified the Mtm1p carrier as the Mn importer into the mitochondrial matrix because its inactivation led to reduced Mn SOD activity and was rescued by supplying the cells with a large amount of Mn (Luk et al., 2003). However, the function of Mtm1p was subsequently reassigned to the control of mitochondrial Fe homeostasis via the import of an enzymatic cofactor that plays a key role in heme biosynthesis (Whittaker et al., 2015). Because the yeast Mtm1p mutant *mtm1*Δ accumulates Fe in its mitochondria, mis-metallation of SOD2 occurs, leading to its inactivation unless the cells are treated with high levels of Mn (Yang et al., 2006). At-MTM1, a likely ortholog of Mtm1p, has been identified in Arabidopsis (Su et al., 2007). No Mn transporter has yet been identified on the chloroplast envelope, but a thylakoid transporter has recently been reported. PHOTOSYNTHESIS AFFECTED MUTANT71 is required for the incorporation of Mn into the oxygen evolving complex of PSII, presumably by transporting Mn into the thylakoid lumen (Schneider et al., 2016).

Mn trafficking into the secretory pathway appears to fulfill important functions in maintaining Mn homeostasis in all kingdoms. Members of the P_{2A}-type ATPase family were shown to function as Ca^{2+}/Mn^{2+} pumps in several organisms. Among these, yeast Pmr1p transports Mn into Golgi-like compartments and its inactivation leads to Mn accumulation in the cytosol, causing Mn toxicity (Rudolph et al., 1989). Two Pmr1p homologs in Arabidopsis, ECA1 and ECA3, which are located in the endoplasmic reticulum (ER) and Golgi, respectively, can rescue *pmr1*Δ growth defect under Mn stress. Inactivation of *ECA1* and *ECA3* alters the tolerance of plants to suboptimal Mn conditions (Wu et al., 2002; Mills et al., 2008). Moreover, MTP11, another Mn-CDF member from Arabidopsis, and its barley (*Hordeum vulgare*) homolog Hv-MTP8, are localized in Golgi /PVC compartments where they control plant tolerance to high Mn through a mechanism that may involve vesicular trafficking to the vacuole and/or secretion to the extracellular space (Delhaize et al., 2007; Peiter et al., 2007; Pedas et al., 2014). Finally, Smf2p, an NRAMP family transporter, is also present in the secretory pathway in yeast, although its target compartment (reported as being intracellular vesicles) still awaits formal identification (Luk and Culotta, 2001). Since Smf2p is required for the activity of Sod2p and protein glycosylation, two enzymes that require a Mn cofactor, this transporter was proposed to function in feeding Mn to downstream organelles (Luk and Culotta, 2001).

Among the six NRAMP family members in Arabidopsis, NRAMP1, NRAMP3, and NRAMP4 have been assigned a function in Mn or Mn/Fe transport (Curie et al., 2000; Thomine et al., 2000; Lanquar et al., 2005, 2010; Cailliatte et al., 2010; Castaings et al., 2016). A fourth member, NRAMP6, has been described as being able to transport Cd, but its physiological function is currently unclear (Cailliatte et al., 2009). In this study, through reverse genetics and functional complementation of yeast mutants, we show that NRAMP2 is an important player in the Mn nutritional pathway in Arabidopsis. Its presence in the endomembrane system is required for adequate distribution of Mn between cell compartments, which is crucial for optimal PSII activity and for controlling reactive oxygen species production.

RESULTS

NRAMP2 Knockdown Mutants Are Hypersensitive to Mn Deficiency

To investigate the role of NRAMP2 in Arabidopsis, we used a reverse genetics approach and analyzed a T-DNA insertion mutant line named *nramp2-3* (Figure 1). *NRAMP2* transcript levels in the mutant line, as measured by quantitative RT-PCR, were strongly reduced but still retained at 5 to 10% of wild-type levels, indicating that *nramp2-3* is a weak allele of *NRAMP2* (Figures 1A and 1B). A second mutant allele of *NRAMP2*, named *nramp2-4*, showed 40% residual *NRAMP2* transcript levels (Figures 1A and 1B). Therefore, both *nramp2-3* and *nramp2-4* are knockdown alleles of *NRAMP2*. Since NRAMP family members have been selected throughout evolution to transport Fe, Mn, or both, we searched for Fe and/or Mn homeostasis defects in the *nramp2* mutants. Fe-limited or excess conditions did not affect the growth of the *nramp2* mutants. In contrast, Mn limitation significantly altered the growth of *nramp2-3*, and to a lesser extent that of *nramp2-4* (Figure 1C; Supplemental Figures 1A and 1B), affecting the root more than the shoot (Figures 1D and 1E). Mn-deficient *nramp2-3* plants harbored moderately chlorotic leaves (Figure 1C; Supplemental Figures 1A, 1B, and 1D). Measurement of the leaf SPAD index revealed a 44% reduction in chlorophyll content in Mn-deficient *nramp2-3* plants (Supplemental Figure 1C). Mn addition to the hydroponic solution rescued the growth defect of *nramp2-3* and partially restored its chlorophyll content (Figures 1D and 1E; Supplemental Figures 1C and 1D). Complemented *nramp2* lines were generated by overexpressing a GFP-tagged version of *NRAMP2* under the control of the *UBIQUITIN10* promoter (*ProUB10:NRAMP2-GFP*) in the *nramp2-3* mutant background (Figure 1B). Two of the complemented lines obtained, named OxNR2 #3 and OxNR2 #6, which overexpressed *NRAMP2* 12- and 8-fold, respectively (Figure 1B), showed full reversion of the *nramp2-3* phenotype in Mn-deficient growth conditions (Figures 1C to 1E). Altogether, these data demonstrate that decreasing *NRAMP2* expression results in hypersensitivity of the plant to Mn deficiency, which suggests that NRAMP2 plays a role in Mn homeostasis.

We next measured Mn contents in shoots and roots of the *nramp2-3* mutant and complemented lines (Figure 2). Under Mn-replete conditions, both mutant and overexpressor lines accumulated significantly higher levels of Mn in shoots and roots than the wild type (Supplemental Table 1). Upon Mn shortage, Mn levels

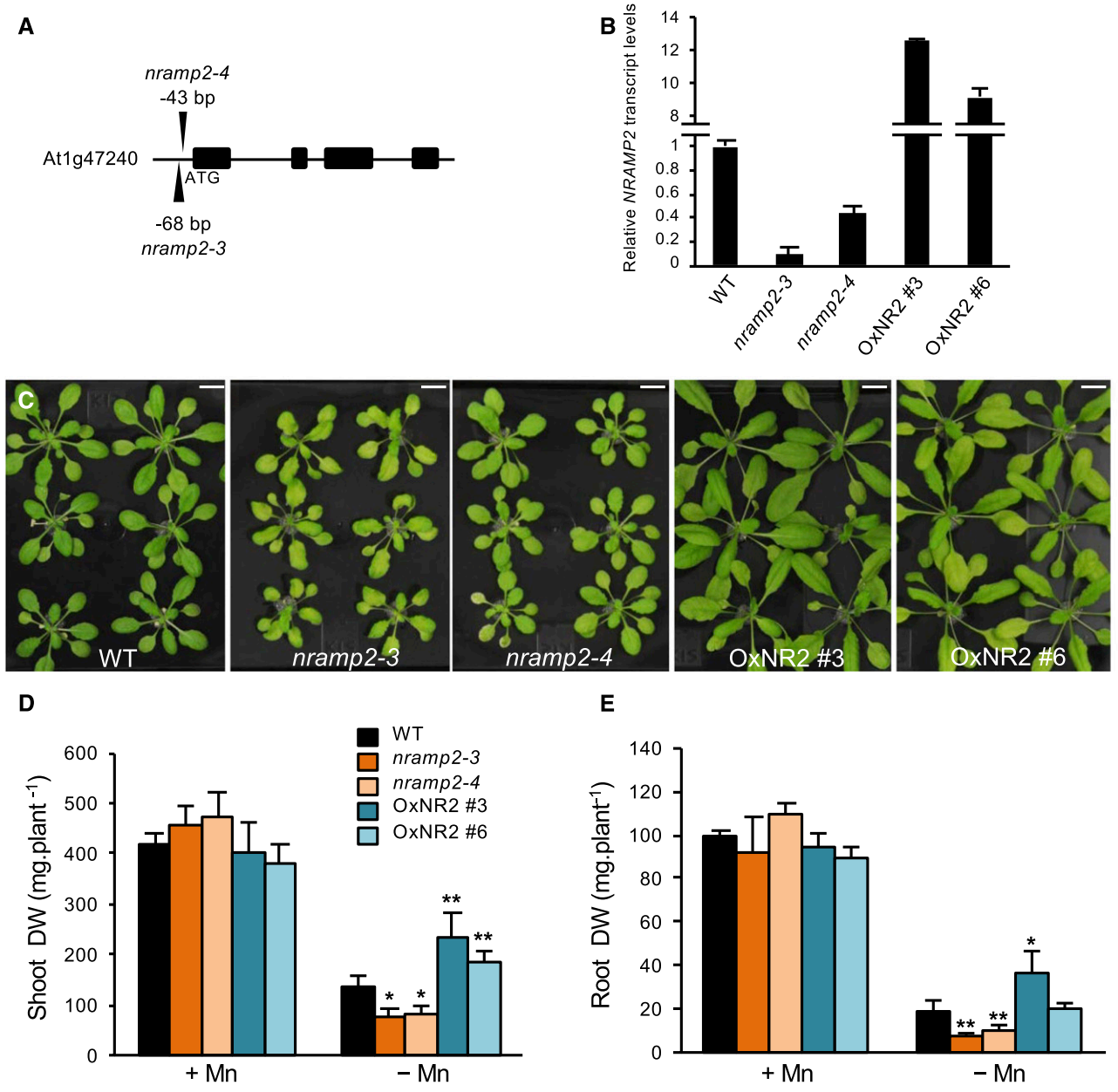

Figure 1. *nramp2* Mutants Are Hypersensitive to Mn Deficiency.

(A) Position of the T-DNA insertion in two *nramp2* mutant alleles relative to the ATG start codon.
(B) Relative *NRAMP2* transcript abundance measured by qRT-PCR in *nramp2* mutant alleles and in the two *nramp2-3* complemented lines OxNR2 #3 and OxNR2 #6. Transcript levels are expressed relative to those of the reference gene *ACTIN* ±SD (n = 3 measurements per sample).
(C) Phenotypes of plants of the indicated genetic backgrounds grown for one week in Mn-replete conditions (5 μM Mn SO_4) followed by three additional weeks in Mn-free hydroponic conditions. Bars = 1 cm.
(D) and **(E)** Shoot **(D)** and root **(E)** biomass production of the plants presented in **(C)**. Data are from one representative experiment (n = 10 plants). **(D)** and **(E)** share color code legends. Mean ± SD. Asterisks indicate values significantly different from those of the wild type (Student's t test, *P value < 0.05 and **P value < 0.01). DW, dry weight.

in the tissues of the mutant were not reduced. Instead, the Mn content increased by 26% in shoots of the *nramp2-3* mutant, a defect that was fully rescued in the two complemented lines (Figure 2; Supplemental Table 1). This result therefore ruled out the possibility that NRAMP2 functions in the acquisition of Mn from the growth medium. We next tested whether an increase in *NRAMP1* expression in roots could account for the high level of Mn in the *nramp2-3* mutant subjected to Mn deficiency. However, the accumulation of *NRAMP1* transcripts was not significantly modified in *nramp2-3* roots in response to Mn deficiency (Supplemental Figure 2).

NRAMP2 Expression Is Ubiquitous in the Plant

We previously showed that *NRAMP2* is expressed in roots and to a lesser extent in shoots (Curie et al., 2000). To examine the response of *NRAMP2* to Mn nutrition, plants were grown in hydroponic conditions for 4 weeks including, or not, a 3-week period of Mn deficiency (Figure 3). The results confirmed the higher accumulation of *NRAMP2* transcripts in roots (Figure 3A). Moreover, the expression of *NRAMP2* was induced ~2.5-fold in response to Mn deficiency both in roots and shoots compared with the control (Figure 3A).

To assess more precisely the localization of *NRAMP2* expression in plant tissues, we generated transgenic plants carrying the GUS reporter gene under the control of the *NRAMP2* promoter. Histochemical analysis of GUS activity showed staining in vascular tissues of roots, cotyledons, and leaves as well as in trichomes of young aerial tissues (Figure 3B, panels a to c). In roots, staining was restricted to the stele, initiating in the elongation zone and strengthening in older parts of the root (Figure 3B, panel d). Cross sections through the root revealed preferential expression in the pericycle (Figure 3B, panel e). In addition, transcriptional profiling in isolated root cell layers (Dinneny et al., 2008) also revealed lower but significant *NRAMP2* expression in epidermis and cortex, particularly close to the root tip (http://www.bar.utoronto.ca/efp/cgi-bin/efpWeb.cgi).

NRAMP2 Is Localized in the TGN Compartment

In order to identify the target membrane of NRAMP2, we investigated the localization of NRAMP2-GFP in complemented lines OxNR2 #3 and #6 expressing *ProUB10:NRAMP2-GFP* (Figure 4). GFP fluorescence, as observed by confocal imaging of root cells of 5-d-old plants, appeared as dot-like structures throughout the cytoplasm, with no labeling of the plasma membrane, which was exclusively labeled with the endocytic tracer FM4-64 (Figure 4A). This fluorescence pattern was unchanged under different Mn regimes. Kinetic analysis of the uptake of FM4-64 revealed partial colocalization of FM4-64 with NRAMP2-GFP after 15 min of treatment (Figure 4B), thus indicating that NRAMP2 localizes to the endomembrane system. To identify the compartment labeled by NRAMP2-GFP, *ProUB10:NRAMP2-GFP* was coexpressed with a set of organelle markers either by transient expression in tobacco (*Nicotiana tabacum*) or through outcrossing with stably transformed Arabidopsis marker lines. The two expression systems produced an identical pattern of fluorescence for NRAMP2-GFP (Supplemental Figures 3A and 3B). No significant colocalization was observed between NRAMP2-GFP and the peroxisomal marker px-rk CD3-983 (Supplemental Figures 3C and 3F). NRAMP2-GFP colocalized partially with the Golgi marker SYP32 (Supplemental Figures 3D and 3G), and with the endosomal marker Rab A1g (Supplemental Figures 3E and 3H).

To narrow down the localization of NRAMP2 within the endomembrane system, *ProUB10:NRAMP2-GFP* was coexpressed with markers of subcompartments of the Golgi apparatus in tobacco leaves. NRAMP2-GFP was in all instances closely associated, but never colocalized, with *cis*- and *trans*-Golgi markers ERD2 and sialyl transferase (ST), respectively (Figure 4C). Since NRAMP2-GFP was systematically distal to the ST-RFP *trans*-Golgi marker (Figure 4C), we suspected that it was localized to the *trans*-Golgi Network (TGN) compartment. Indeed, NRAMP2-GFP showed near-perfect colocalization with the TGN marker SYP61-RFP (Figure 4D). Pearson correlation coefficients and Mander's overlap coefficients above thresholds were calculated for NRAMP2-GFP with either the marker ERD2-CFP, ST-RFP, or RFP-SYP61 and confirmed the overlap between NRAMP2 and SYP61 proteins (Supplemental Table 2). Therefore, NRAMP2 is a protein of the endosomal network predominantly located in the TGN.

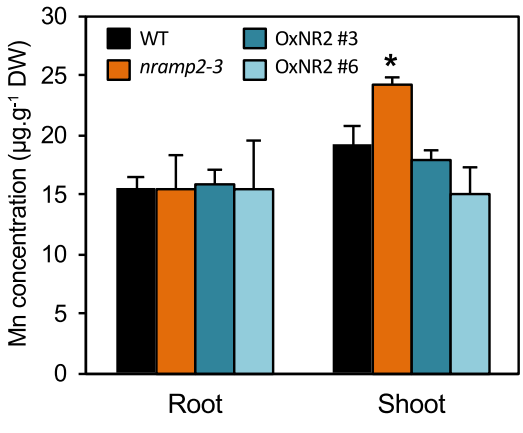

Figure 2. *nramp2-3* Shows Mn Homeostasis Defects under Mn-Free Conditions.

Mn content in the Mn-deficient plants presented in Figure 1 and in control plants grown in parallel in Mn-replete conditions shown in Supplemental Figure 1D. Data are from one representative experiment ($n = 4$ plants). DW, dry weight. Mean ± SD. Asterisks indicate values significantly different from those of the wild type (Student's t test, *P value < 0.01).

Characterization of the Role of NRAMP2 in Mn Transport by Heterologous Expression Analysis in Yeast

To obtain insight into the Mn transport activity of NRAMP2, we tested its ability to functionally complement yeast mutants inactivated in various Mn transport systems (Figure 5). The yeast NRAMP homolog Smf1p, which mediates Mn uptake at the plasma membrane (Supek et al., 1996), was investigated first. Growth of the *smf1*Δ mutant, which is reduced in the presence of EGTA due to Mn limitation, was not restored by the expression of Arabidopsis *NRAMP2* (Figure 5A), unlike what was observed with Arabidopsis *NRAMP1* (Curie et al., 2000; Thomine et al., 2000). We also previously showed that unlike NRAMP1, NRAMP2 did not complement the plasma membrane iron uptake defect of the *fet3*Δ*fet4*Δ mutant (Curie et al., 2000). Therefore, NRAMP2 is unlikely to perform uptake at the plasma membrane, a result that is consistent with our finding that NRAMP2 is located in an intracellular compartment and that Mn acquisition is not affected in the *nramp2* mutant. Since Smf2p in yeast had been described as an endomembrane Mn transporter (Cohen et al., 2000), we tested whether NRAMP2 could functionally replace Smf2p. Growth of *smf2*Δ, which like *smf1*Δ is reduced in the presence of EGTA, was fully restored by the expression of *NRAMP2* (Figure 5A). Phenotypes of *smf2*Δ also include a strong decrease in cellular Mn

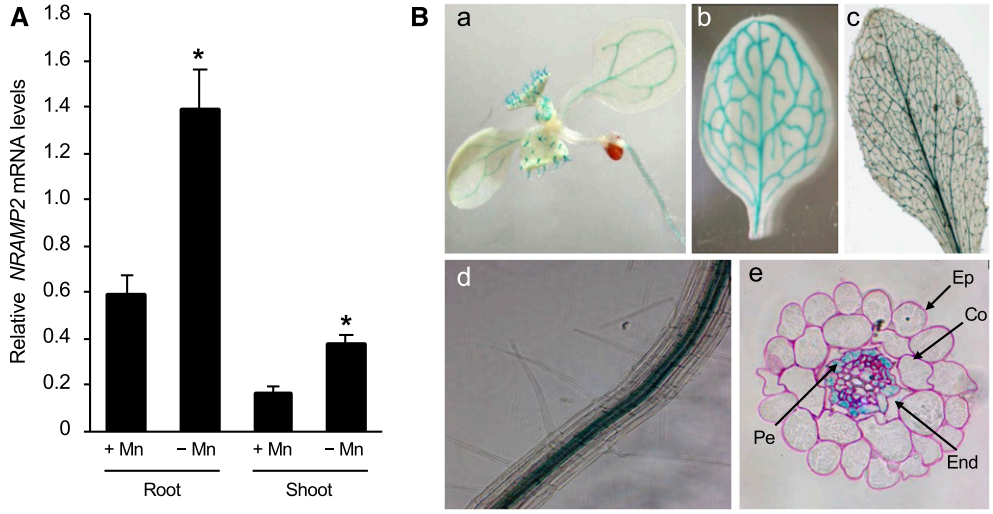

Figure 3. *NRAMP2* Expression Analysis.

(A) Relative *NRAMP2* transcript abundance in roots and shoots measured by qRT-PCR. Transcript levels are expressed relative to those of the reference gene *ACTIN* ±SD ($n = 3$ technical replicates). Wild-type plants were grown hydroponically for 3 weeks in control (5 μM $MnSO_4$) or in Mn-free (−Mn) conditions. Data are from one representative experiment ($n = 3$ plants). Mean ± SD. Asterisks indicate values significantly different from those of control conditions (Student's *t* test, *P value < 0.01).

(B) Histochemical staining of GUS activity in *proNRAMP2:GUS*-transformed Arabidopsis grown in Mn-replete conditions. **(a)** Six-day-old seedling; **(b)** young rosette leaf; **(c)** mature rosette leaf; **(d)** Primary root of a 1-week-old plant in the mature zone; **(e)** root cross section in the mature zone. Ep, epidermis; Co, cortex; End, endodermis; Pe, pericycle. Data are shown for one representative line out of three independent lines.

content and Mn SOD activity (Luk and Culotta, 2001). As expected, NRAMP2 restored both the Mn content and Mn SOD activity of *smf2*Δ (Figures 5B and 5C), suggesting that NRAMP2 is a true ortholog of the yeast Smf2p intracellular Mn transporter.

We also tested the capacity of NRAMP2 to rescue *pmr1*Δ, a yeast mutant lacking the Mn transport ATPase for the Golgi. *pmr1*Δ is hypersensitive to high Mn due to increased Mn accumulation in the cytosol. The expression of *NRAMP2* did not rescue the *pmr1*Δ phenotype (Figure 5E). This finding suggests that NRAMP2 activity does not reduce cytosolic Mn concentrations, which in turn implies that it mediates Mn import into the cytosol. Interestingly, we found that NRAMP2 also efficiently rescued the sensitivity of *mtm1*Δ to EGTA (Figure 5D). *mtm1*Δ was shown to misincorporate Fe instead of Mn into mitochondrial SOD and can be rescued by supplying excess Mn to the cell (Yang et al., 2006; Whittaker et al., 2015). Since NRAMP2 is a protein in the TGN membrane, its ability to rescue *mtm1*Δ supports a role for this protein in improving cellular Mn availability.

PSII Activity Is Reduced in the *nramp2-3* Mutant Exposed to Mn Starvation

Since a cluster of four Mn atoms is associated with the oxygen-evolving complex of PSII, we searched for defects of photosynthesis activity in the *nramp2-3* mutant that could explain its slow growth under Mn deficiency. We measured a number of photosynthesis parameters, including maximal photochemical efficiency of PSII (Fv/Fm) and PSII operating efficiency (Φ_{PSII}). The Fv/Fm values (close to 0.8) were unchanged for all genotypes grown under control conditions (Figure 6, left panel). Under Mn limitation, the Fv/Fm value decreased by 30% in wild-type plants, thereby highlighting the requirement of Mn for PSII activity, and noticeably dropped by an additional 10% in leaves of the *nramp2-3* (Figure 6, right panel; Supplemental Table 3) and *nramp2-4* mutants (Supplemental Table 3). This phenotype was rescued in the two OxNR2-complemented lines (Figure 6, right panel; Supplemental Table 3). Thus, NRAMP2 is required to maintain optimal PSII activity in conditions of limited Mn availability. Electron transfer flow downstream of PSII, which is estimated by the Φ_{PSII} value, was also more dramatically reduced under Mn-deficient conditions in the two *nramp2* mutants compared with wild-type plants and was restored to a higher value than the wild type in the OxNR2-complemented lines (Supplemental Table 3). Therefore, photosynthesis efficiency under Mn-deficient conditions requires an active NRAMP2.

The Growth Defect of the *nramp2* Mutant Is Associated with Reduced Mn Levels in Chloroplasts and Vacuoles

To refine the role of NRAMP2 in the mobilization of internal Mn pools, Mn content was measured in protoplasts and subcellular fractions of the wild type, *nramp2-3*, and the OxNR2 #3-complemented line grown in either Mn-replete or Mn-deficient conditions (Figure 7; Supplemental Table 4). In Mn-starved *nramp2-3* plants that display a strong phenotype, total Mn content remained unchanged in protoplasts compared with protoplasts isolated from wild-type plants (Figure 7A). This confirmed that inactivation of NRAMP2 affects the intracellular distribution of Mn rather than total cellular content. We next tested whether the reduced photosynthesis activity measured in *nramp2-3* was

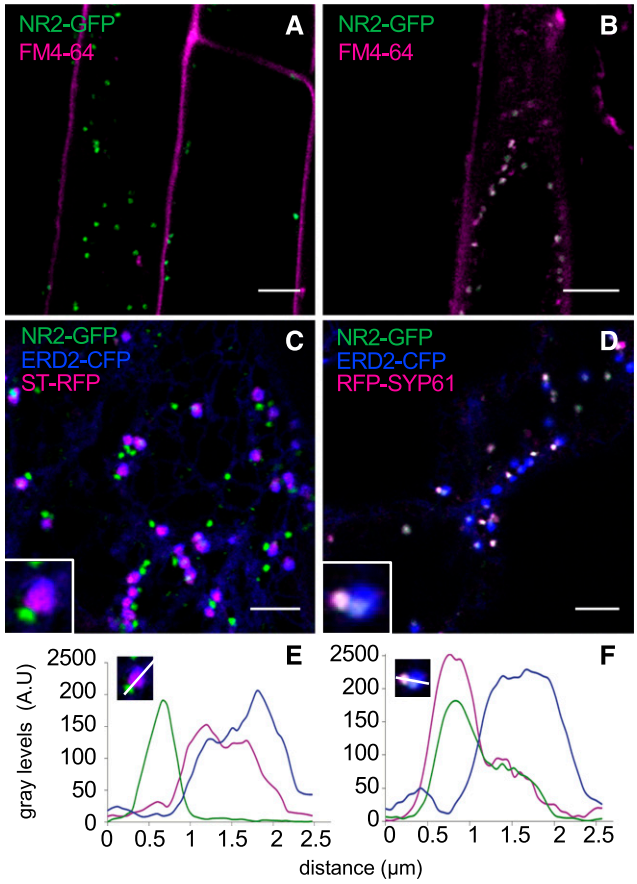

Figure 4. NRAMP2 Is Localized to the TGN.

(A) and **(B)** Fluorescence pattern of the NRAMP2-GFP construct and kinetics of colocalization with the endocytic tracer FM4-64 (**[A]** 2 min; **[B]** 15 min) observed by confocal microscopy in roots of 5-d-old plants.

(C) and **(D)** Colocalization of NRAMP2-GFP with markers for *cis*-Golgi (ERD2-CFP), *trans*-Golgi (ST-RFP), and TGN (SYP61-GFP) transiently coexpressed in tobacco leaves. Inserts show a close-up image of the association of NRAMP2-GFP with the various Golgi subcompartments. Bars = 5 μm.

(E) and **(F)** Pixel intensity profiles of GFP (green), RFP (magenta), and CFP (blue) were measured along a line spanning the subcompartments magnified in the close-up insets shown in **(C)** and **(D)**, respectively.

associated with a lower Mn content in the chloroplasts. Under Mn deficiency, the Mn concentration dropped almost 2-fold in the chloroplasts of *nramp2-3* relative to wild-type plants, a defect that was rescued in the OxNR2 #3 line (Figure 7B). This suggested that reduced PSII activity in Mn-deficient *nramp2-3* plants is caused by the lesser availability of Mn in the chloroplasts. Vacuoles were also isolated from the same protoplasts in order to test for a general defect of Mn content in organelles. Indeed, *nramp2-3* vacuoles showed reduced Mn concentration (Figure 7C), confirming that NRAMP2 is required to maintain optimal Mn concentration in several organelles. We therefore concluded that under Mn deficiency, NRAMP2 contributes to building up an available pool of cellular Mn to be used by downstream compartments including, but most likely not restricted to, chloroplasts and vacuoles.

Cellular Redox Homeostasis Is Disturbed in the *nramp2* Mutant

The second prime target of Mn deficiency in plants is the mitochondrial superoxide dismutase, or Mn SOD, the function of which is affected in the yeast *smf2*Δ mutant (Luk and Culotta, 2001; this work). To test whether Mn SOD activity is affected in the *nramp2* mutant, an in-gel SOD activity assay was performed (Figure 8). Despite the prolonged Mn starvation treatment imposed in this experiment, Mn SOD activity remained unaffected regardless of the genotype (Figure 8A). These data indicate that in contrast to PSII, Mn SOD activity is maintained in the *nramp2* mutant under Mn-deficient conditions. The most striking change was observed for Cu/Zn SOD, the activity of which was strongly enhanced in *nramp2* plants grown in Mn-limiting conditions (Figure 8A). Complementation of the mutant with NRAMP2 efficiently normalized the activity of Cu/Zn SOD (Figure 8A). A slight increase in Fe SOD activity was also observed in Mn-deficient *nramp2-3* plants; however, contrary to Cu/Zn SOD, Fe SOD activity was not rescued in the two OxNR2-complemented lines (Figure 8A).

The enhanced activity of Cu/Zn SOD revealed an imbalance of the redox status in Mn-deficient *nramp2* cells. We thus monitored the production of reactive oxygen species in the *nramp2* mutant, especially the superoxide anion ($O_2 \cdot^-$), which is the substrate of Cu/Zn SOD. In situ detection of $O_2 \cdot^-$ ions was performed by staining mature leaves with nitroblue tetrazolium (NBT). Leaves of the *nramp2-3* mutant showed strong purple NBT staining regardless of the Mn regime, a phenotype that was mostly reverted in the OxNR2 #3-complemented line (Figure 8B). Increased NBT staining was not observed in the *nramp3 nramp4* double mutant (Figure 8B), even though this mutant shared several Mn-related phenotypes with *nramp2* when exposed to Mn deficiency, including a growth defect and an alteration of Mn homeostasis in chloroplasts (Lanquar et al., 2010).

In parallel, we tested whether NRAMP2 could rescue the oxidative stress of the *sod1*Δ yeast mutant defective in cytosolic Cu/Zn SOD. *sod1*Δ showed sensitivity to as low as 1 mM EGTA, a phenotype that was fully rescued by the expression of *NRAMP2* (Figure 8C). This indicated that the pool of Mn displaced by NRAMP2 can efficiently replace cytosolic SOD activity in yeast. Altogether, these results support the view that the Mn transport activity of NRAMP2 takes part in the cellular antioxidant pathway.

Leaf Surface Permeability Is Affected in the *nramp2-3* Mutant

Mn-starved *nramp2-3* plants displayed somewhat low turgor in leaves. A relationship between tissue Mn content and cuticular wax synthesis in leaves has previously been pointed out but is not well documented (Wilson et al., 1982; Hebbern et al., 2009). We therefore investigated the permeability of the leaf surface in the *nramp2-3* mutant under Mn-replete or -deficient conditions (Figure 9). The integrity of the leaf cuticle can be revealed by staining with an aqueous solution of the hydrophilic dye Toluidine blue (TB) (Tanaka et al., 2004). TB-exposed rosette leaves of the *nramp2-3* mutant showed an irregular punctuate staining after 10 min that contrasted with the intact cuticles of wild-type and OxNR2 #3 leaves, suggesting that the cuticles are permeable in

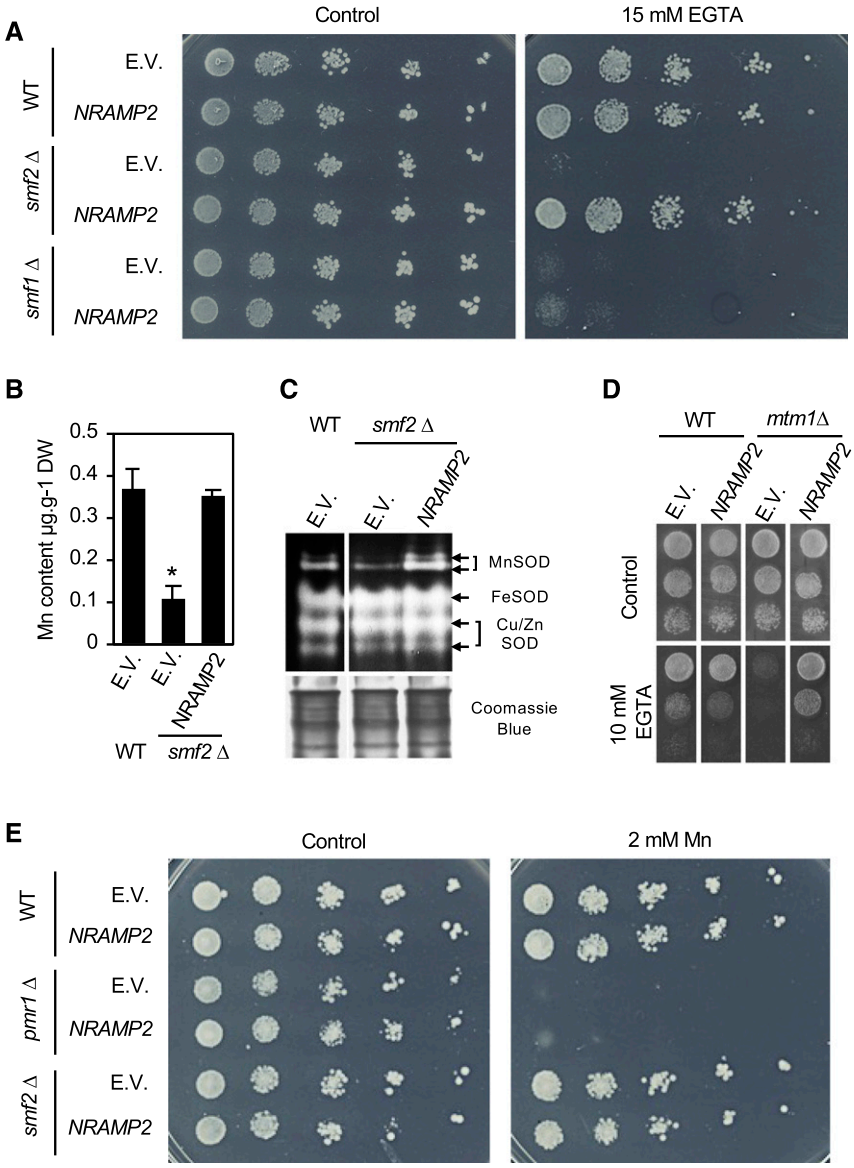

Figure 5. NRAMP2 Complements the *smf2*Δ and *mtm1*Δ Yeast Mutants.

(A), **(D)**, and **(E)** Growth tests of wild-type (BY4741) and mutant yeast strains *smf1*Δ **(A)**, *smf2*Δ (**[A]** and **[E]**), *mtm1*Δ **(D)**, and *pmr1*Δ **(E)** transformed with the pYPGE15 empty vector (E.V.) or the pYPGE15/NRAMP2 construct (*NRAMP2*). Fivefold serial dilutions were plated on SD-Ura supplemented or not (control) with the amount of EGTA indicated in **(A)** and **(D)** or 2 mM $MnSO_4$ **(E)** and incubated at 30°C for 3 d.

(A) NRAMP2 restores *smf2*Δ mutant tolerance to Mn deficiency.

(B) Mn content measured by MP-AES in yeast strains grown in liquid SD -URA for 24 h. Mean ± SD ($n = 3$). Asterisks indicate values significantly different from those of the wild type (Student's *t* test, *P value < 0.01).

(C) In-gel SOD activity assay performed on proteins extracted from yeast strains grown as in **(B)**.

(D) NRAMP2 restores *mtm1*Δ mutant tolerance to Mn deficiency.

(E) NRAMP2 fails to rescue *pmr1*Δ mutant sensitivity to excess Mn and does not reduce wild-type or *smf2*Δ tolerance to excess Mn.

nramp2-3 leaves (Figure 9A). By contrast, the *nramp1-1* mutant, whose Mn content is strongly reduced under Mn deficiency (Cailliatte et al., 2010), showed the same intensity of TB staining as wild-type leaves (Supplemental Figure 4). This suggested that, rather than Mn deficiency, it is the adequate allocation of Mn in cell compartments that is crucial for producing leaf surface components. Finally, we measured the cutin content in the leaves of *nramp2-3*- and *NRAMP2*-complemented line OxNR2 #3 (Figure 9B; Supplemental File 1). Upon Mn deficiency, the cutin load was reduced by 40% in wild-type plants, indicating that Mn is required for the production of an intact cuticle in Arabidopsis leaves. Cutin content was unchanged in the *nramp2-3* mutant in control

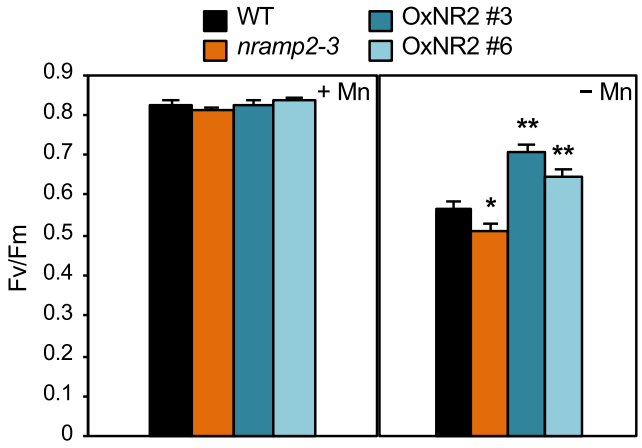

Figure 6. Photosynthetic Activity Is Impaired in *nramp2-3*.

Maximum PSII efficiency (F_v/F_m) measured on rosette leaves of the wild type, *nramp2-3*, and two complemented lines grown for 4 weeks in hydroponic conditions in the presence of Mn (+Mn) or 1 week with Mn and transferred to medium without Mn for three additional weeks (−Mn). Mean ± SD (n = 10 leaves from 10 plants). Asterisks indicate values significantly different from those of the wild type (Student's t test, *P value < 0.05 and **P value < 0.01).

condition, but when exposed to Mn deficiency, *nramp2-3* was more severely affected than wild-type plants, showing a more than 70% decrease. Consistent with TB staining, this phenotype of *nramp2-3* in Mn-deficient conditions was rescued in the OxNR2 #3-complemented line. Taken together, these results indicate that Mn compartmentalization by NRAMP2 plays an important role in assembling the leaf cuticle in Arabidopsis.

Genetic Interaction between NRAMP2 and the Tonoplastic NRAMP Members NRAMP3 and NRAMP4

Hypersensitivity to Mn deficiency, reduced Mn content in chloroplasts, and decreased photosynthesis activity are features that are reminiscent of the phenotype of the *nramp3 nramp4* double mutant. We therefore tested functional redundancy between NRAMP2 on one hand, and NRAMP3 and NRAMP4 on the other hand, by crossing the *nramp2* and *nramp3 nramp4* mutants. The triple *nramp2 nramp3 nramp4* mutant did not exhibit higher sensitivity to Mn deficiency than the two parental lines, as shown by the equivalent reduction in photosynthetic activity in all of these mutants (Supplemental Table 5). This suggested that the three transporters act in the same pathway to provide Mn to the chloroplasts. Furthermore, superoxide production was enhanced in the *nramp2 nramp3 nramp4* triple mutant, as observed in *nramp2* (albeit seemingly less so) but not in *nramp3 nramp4*, thus indicating that *NRAMP2* is epistatic to *NRAMP3*/*NRAMP4* (Supplemental Figure 5).

DISCUSSION

In this study, we characterized the phenotypic changes in Arabidopsis plants carrying a knockdown allele of *NRAMP2*. NRAMP2 is a protein localized in the TGN membrane that can functionally replace the yeast endomembrane Mn transporter Smf2p. The *nramp2* mutant displays pleiotropic defects that are exacerbated in Mn-deficient conditions and that collectively point to a role of the NRAMP2 transporter in the intracellular distribution of Mn to its target compartments.

Mn Is a Physiological Substrate for NRAMP2

Our study provides strong, although indirect, arguments in favor of NRAMP2 acting as an Mn transporter. The strongest argument is its ability to rescue the growth of a yeast mutant with an inactivated *SMF2* gene, which encodes an NRAMP homolog with reported Mn transport activity. NRAMP2 can fully substitute for Smf2p, since its expression not only restored the growth of the *smf2*Δ mutant in Mn-limiting conditions, but it also rescued its defective Mn SOD activity, suggesting that NRAMP2 is a true ortholog of yeast Smf2p. In addition, we obtained evidence that NRAMP2 functions as a Mn transporter in planta. We found that *NRAMP2* knockdown plants exhibited impaired growth, specifically in Mn-limiting conditions, whereas *NRAMP2*-overexpressing lines show

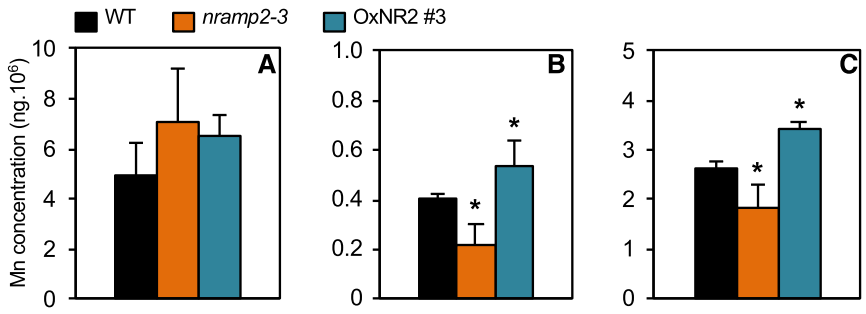

Figure 7. Vacuoles and Chloroplasts of the *nramp2-3* Mutant Contain Less Mn Than the Wild Type.

Mn content was measured on isolated protoplasts **(A)**, chloroplasts **(B)**, or vacuoles **(C)** in the wild type, *nramp2-3*, and the OxNR2 #3-complemented line grown in hydroponic cultures for 1 week in the presence of Mn followed by three additional weeks in the absence of Mn. All panels share color code legends. Metal concentration was determined by MP-AES and is expressed as nanograms per 10^6 protoplasts or organelles. Data are from one representative experiment (n = 4 plants). Mean ± SD. Asterisks indicate values significantly different from those of the wild type (Student's t test, *P value < 0.01).

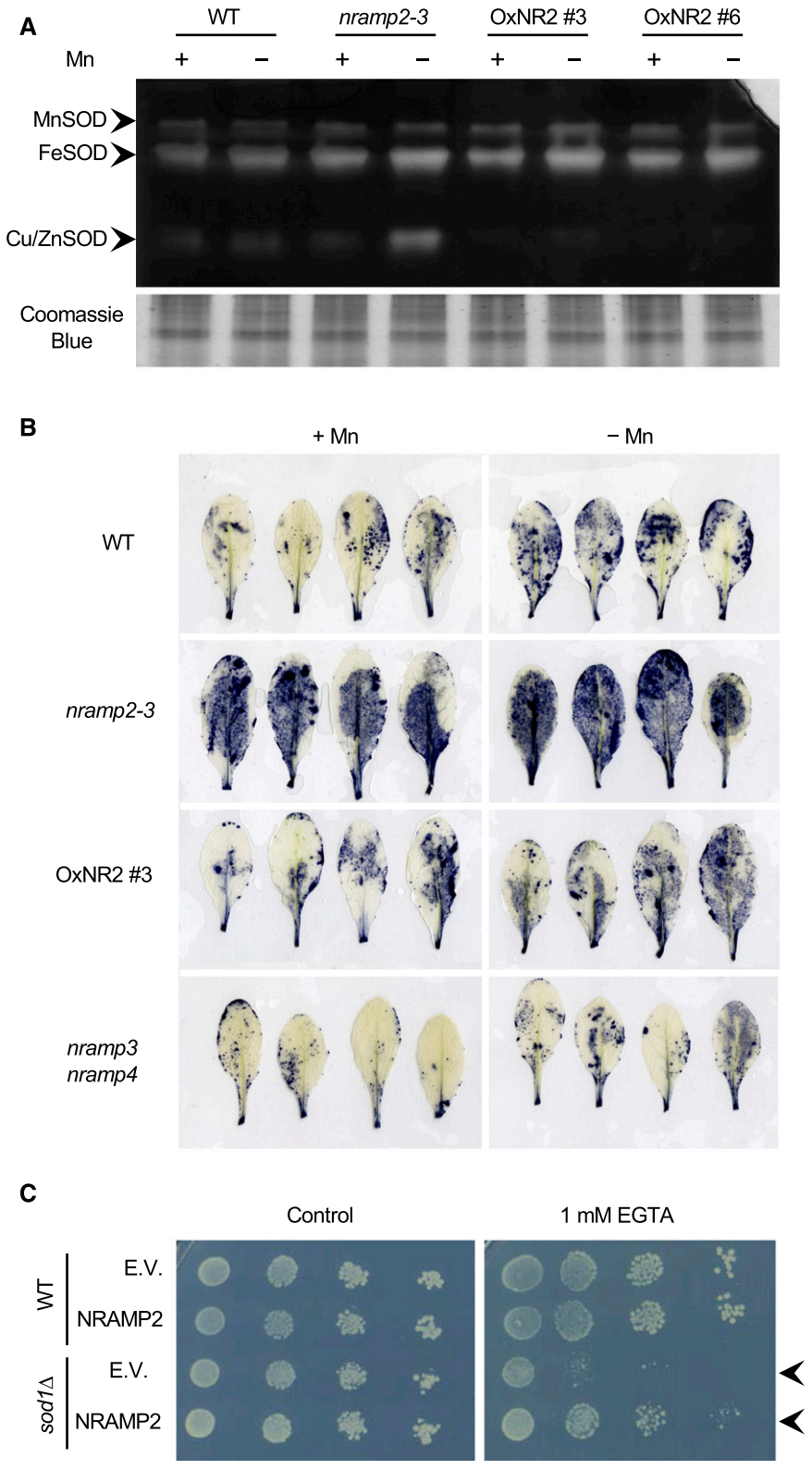

Figure 8. *nramp2-3* Displays High Levels of Oxidative Stress.

(A) and **(B)** Plants of the indicated genotypes were cultivated in hydroponic conditions for 4 weeks in the presence of Mn (+Mn) or 1 week with Mn and transferred to medium without Mn for three additional weeks (−Mn).

(A) In-gel SOD activity assay performed using total proteins extracted from leaves.

(B) Detection of superoxide ion production in Mn-replete or Mn-starved leaves by staining with NBT.

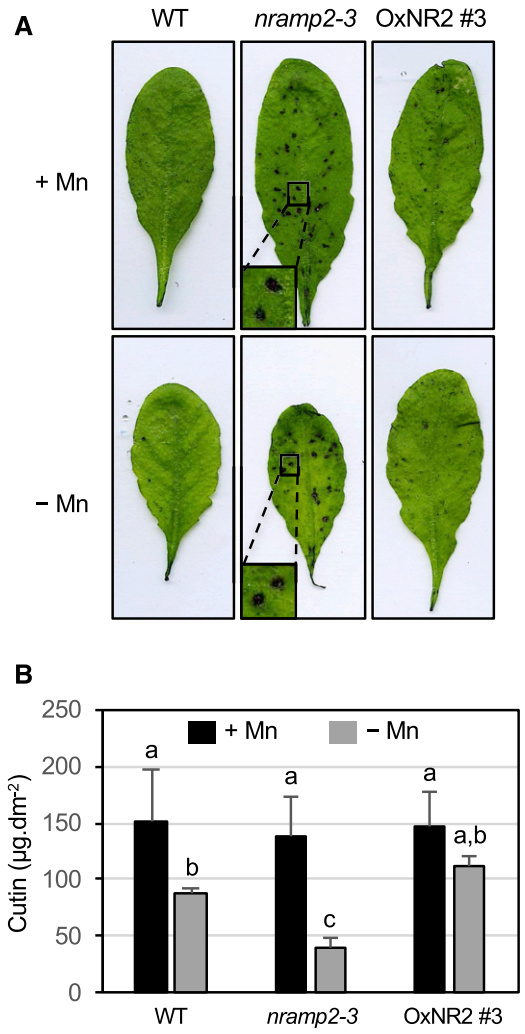

Figure 9. *nramp2-3* Shows Cell Wall Permeability Defects.

Plants of the indicated genotypes were grown in hydroponic conditions for 3 weeks in the presence of Mn followed by an additional week in the presence (+Mn) or absence of Mn (−Mn).

(A) Permeability of the leaf surface was examined by staining entire leaves with TB for 10 min. Insets show a close-up view of the TB-stained spots on the leaves.

(B) Cutin load per surface unit of leaf measured by gas chromatography-mass spectrometry. Mean ± SD ($n = 4$ leaves from four plants). Values that are not significantly different are noted with the same letter (ANOVA, α risk 5%; Supplemental File 1).

hypertolerance to this treatment. Furthermore, the Mn content in two cellular compartments, vacuoles and chloroplasts, was markedly reduced in the *nramp2* mutant. Lastly, *NRAMP2* gene expression was induced in response to Mn deficiency, which supports its involvement in Mn homeostasis. Thus, out of the six NRAMP transporters in Arabidopsis, NRAMP2 represents the fourth member to play a major role in Mn transport, next to NRAMP1, NRAMP3, and NRAMP4. The same observation holds true for the characterized rice Os-NRAMP members and might be a general feature of plant NRAMPs, thus distinguishing them from animal NRAMPs, which appear to be more active in Fe transport.

NRAMP2 Is a Resident TGN Protein

Unlike NRAMP1, NRAMP2 failed to rescue the plasma membrane Mn uptake of the yeast Δ*smf1* mutant but successfully substituted for Mn transport by Smf2p, which is located on vesicles of the yeast endomembrane system (Portnoy et al., 2000; Luk and Culotta, 2001). We therefore made the assumption that NRAMP2 works intracellularly in the plant. In plant cells, we found that NRAMP2 localized to a vesicular compartment. Using a set of endomembrane markers, we showed that NRAMP2 primarily colocalized with the TGN marker SYP61. Since endocytosed plasma membrane proteins are initially targeted to early endosomes, and since the TGN can also function as an early endosome in plants (Uemura and Nakano, 2013), a possibility existed that NRAMP2 was in fact cycling between the plasma membrane and TGN. Interestingly, dual targeting of NRAMP1 between the plasma membrane and intracellular vesicles of the endomembrane pathway was recently reported (Agorio et al., 2017). Unlike NRAMP1, however, we did not find evidence for the presence of NRAMP2 at the cell surface, regardless of whether NRAMP2-GFP-expressing plants were Mn starved or treated with the endocytosis inhibitor Tyrphostin A23. Consistent with our localization data, NRAMP2, but none of the other Arabidopsis NRAMP isoforms, was identified in a proteomic study performed on affinity purified SYP61-containing TGN vesicles (Drakakaki et al., 2012). Therefore, NRAMP2 is likely a resident TGN protein.

Loss of NRAMP2 Affects Mn Content in Organelles

Our data reveal that PSII activity is severely reduced in leaves of the *nramp2* mutant exposed to Mn deficiency and that this decrease correlates with reduced Mn content in the chloroplasts. This strongly suggests that NRAMP2 helps maintain chloroplastic Mn at an optimal concentration for photosynthetic activity. We established that in addition to chloroplast content, vacuolar Mn content is also significantly reduced in the *nramp2* mutant. Thus, rather than specifically targeting the chloroplast, we suspected that NRAMP2 works upstream of several organelles, probably by functioning at an early crossroad in the distribution pathway. If this was indeed the case, we reasoned that NRAMP2 would likely distribute Mn to most of its target organelles. Consistent with this idea, we found that NRAMP2 complemented the defective growth of the mitochondrial mutant *mtm1*Δ under Mn deficiency, suggesting that NRAMP2 increases Mn availability for this organelle. In Arabidopsis, however, Mn SOD activity, which we used as

Figure 8. (continued).

(C) NRAMP2 rescues the sensitivity of the yeast *sod1*Δ mutant to Mn deficiency. Fivefold serial dilutions were plated on SD-Ura supplemented with 1 mM EGTA (right) or not (Control; left). Arrows indicate the growth rescue of *smf2*Δ by NRAMP2.

a proxy for mitochondrial Mn level, remained unchanged in the *nramp2* mutant, regardless of the Mn regime. This suggests that Mn levels in mitochondria do not rely on the Mn transport activity of NRAMP2 or that an alternative pathway exists that compensates for the absence of NRAMP2. Interestingly, Mn SOD activity in wild-type plants was unaffected by Mn starvation, whereas the same conditions efficiently depleted chloroplast content and affected PSII activity. A similar result was previously reported (Lanquar et al., 2010). This suggests the existence of a hierarchy of Mn allocation to the organelles in which maintaining mitochondrial Mn homeostasis is a priority for the plant. Exactly the opposite result was obtained in *Chlamydomonas reinhardtii*, where loss of activity of Mn SOD precedes the loss of PSII activity (Allen et al., 2007). In conclusion, such a strong mechanism of preservation of Mn SOD activity in Mn-starved Arabidopsis plants likely masks a potential impact of NRAMP2 mutation on mitochondrial Mn content.

The chloroplastic pool of Mn was previously proposed to originate from the vacuole because mutating the tonoplastic Mn transporters NRAMP3 and NRAMP4, which remobilize stored Mn from the vacuoles, led to a decreased concentration of Mn in chloroplasts (Lanquar et al., 2010). The finding that metal content in chloroplasts is tightly linked to the capacity of metal release from the vacuole was further demonstrated in two independent studies. When both the Arabidopsis YSL4 and YSL6 chloroplast transporters were inactivated, which led to increased Fe accumulation in the chloroplasts, the expression of *NRAMP3* and *NRAMP4* was dramatically inhibited, presumably as a feedback mechanism aimed at preventing Fe overload into the chloroplasts (Divol et al., 2013). Furthermore, the steady state level of ferritins, the stability of which depends on the presence of iron in the chloroplast, is drastically reduced in the *nramp3 nramp4* double mutant background (Ravet et al., 2009). Again, these results suggest that a direct link exists between Fe efflux from the vacuole and Fe content in the chloroplasts. Altogether, these studies indicate that at least a large portion of these metals contained in the chloroplasts originates from the vacuoles. Within the pathway that provides Mn to the chloroplasts, several lines of evidence support the idea that the three transporters, NRAMP2, NRAMP3, and NRAMP4, act together, with NRAMP2 operating before the other two: (1) The phenotype of hypersensitivity to Mn deficiency of the *nramp2 nramp3 nramp4* triple mutant is similar in intensity to that of the *nramp2* single mutant; (2) the pleiotropic phenotypes of *nramp2* include all of the alterations of *nramp3 nramp4* but also additional ones such as oxidative stress imbalance, vacuolar Mn depletion, and cuticular wax defects; and (3) *NRAMP2*, *NRAMP3*, and *NRAMP4* have overlapping spatial expression patterns and respond similarly to Mn deficiency. Together, these experiments argue against the direct uptake of Mn from the cytosol and rather favor a strategy by which Mn first accumulates into the vacuole prior to being dispatched to its target organelles. Favoring safe metal storage into the vacuole, from which at least the chloroplast draws part of its supply, may be a strategy used by the plant to prevent toxicity of these reactive metals in the cytosol.

Mn and Leaf Surface Permeability

We demonstrated that leaf surface permeability and cutin production are disturbed specifically in *nramp2-3* plants exposed to Mn deficiency and more generally as a result of Mn starvation. A reduction in the epicuticular layer in response to Mn deficiency was previously described in barley, where it was shown to be associated with a change in transpiration rate and water use efficiency (Hebbern et al., 2009). This transformation, which may partly explain the reported susceptibility of Mn-deficient crops to pathogens, might correspond to an adaptation of the plant to reduced PSII activity. Furthermore, Mn availability was also found to regulate root suberization, resulting in higher permeability of the stele in response to metal shortage (Barberon et al., 2016). Interestingly, whereas both *nramp1* and *nramp2* are Mn starved under conditions of low Mn supply (Cailliatte et al., 2010), only the leaf permeability of *nramp2* was more affected than wild-type plants in these experiments. Thus, it appears as though this phenotype is caused by Mn deficiency in a specific cell compartment rather than by global plant Mn status. Cuticle components are synthesized predominantly in the ER (Yeats and Rose, 2013) and are then thought to be secreted to the cell wall via an ER-Golgi route (Hoffmann-Benning and Kende, 1994). To date, no Mn-dependent enzymatic activity has been identified in the biosynthetic pathway of cuticular components. As is the case for the vacuole, chloroplast, and mitochondria, the availability of Mn to endosomal compartments such as the ER and Golgi apparatus might be reduced in the *nramp2* mutant, hence affecting

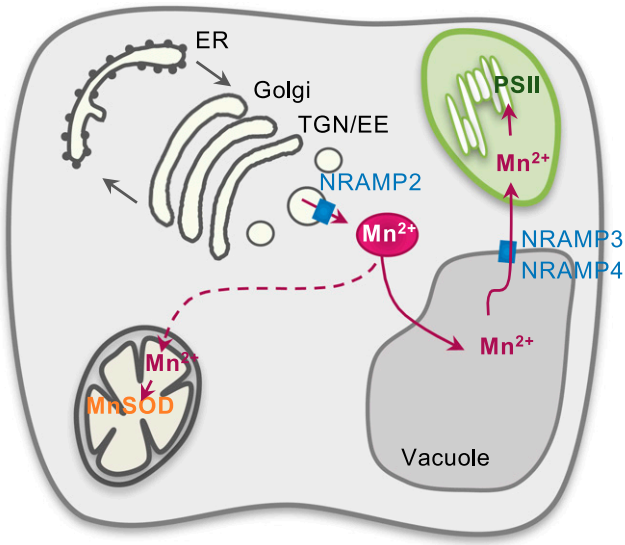

Figure 10. Hypothetical Model of the Function of NRAMP2 in Cellular Mn Distribution.

When NRAMP2 is nearly absent (*nramp2* knockdown mutants), plants are hypersensitive to Mn deficiency and PSII activity is markedly impaired. NRAMP2 is a transporter of the TGN membrane where it likely exports Mn from the TGN lumen to the cytosol. In doing so, NRAMP2 builds up a pool of Mn (red circle) that, based on the pleiotropic effects of the *NRAMP2* mutation, is used to feed an array of downstream organelles: vacuoles and chloroplasts, since both display decreased Mn content in *nramp2-3*, and mitochondria based on the ability of NRAMP2 to complement yeast *mtm1*Δ. Combining *nramp2-3* with *nramp3-2* and *nramp4-2* mutations suggests that NRAMP2 and NRAMP3/NRAMP4 act in concert to provide Mn to the PSII, NRAMP2 being epistatic to the other two.

a potential Mn-containing enzyme involved in cuticle biosynthesis. It is noteworthy that an important class of Mn-containing proteins of the cell is constituted by the large family of glycosyl transferases, which are mainly located in the Golgi, where they glycosylate various substrates, among which are important glycoproteins of the cell wall. Whether NRAMP2 brings Mn to Golgi-localized glycosyl transferases or ER-localized cuticle biosynthetic enzymes deserves further investigation.

Oxidative Stress Level Is Elevated in *nramp2*

The *nramp2* mutant experiences redox imbalance under Mn-deficient conditions based on increased Cu/Zn SOD activity and enhanced O_2^- production. The high O_2^- level in the mutant is likely not provoked by reduced mitochondrial Mn SOD activity, as we found no modification of this activity in *nramp2*, thus ruling out mitochondria as a source of O_2^-. Since we measured increased Cu/Zn SOD, we speculated that O_2^- radicals produced by *nramp2* originate from defective photosynthesis. Yet, the *nramp3 nramp4* double mutant, which also displays reduced Mn content in chloroplasts and impaired F_v/F_m activity (Lanquar et al., 2010), shows no defect in redox homeostasis. Therefore, the observation that only *nramp2* plants showed higher oxidative stress levels strongly suggests that the localization of NRAMP2 in the TGN, and therefore intracellular management of Mn pools, is central to the cellular redox imbalance of the mutant.

In yeast, small molecular weight Mn complexes in the cytosol display SOD activity, thereby acting as an alternative, parallel system to enzymatic SODs and providing an explanation for the rescue of *sod1*Δ by Smf2p (McNaughton et al., 2010). We found in this work that Arabidopsis NRAMP2 too can compensate for the absence of Sod1p in yeast. The role of Mn-Pi or Mn^{2+} complexes with small organic molecules as potent scavengers of superoxide has also been revealed in bacteria, and evidence that such antioxidant Mn species exist in multicellular organisms was recently obtained in *Caenorhabditis elegans* and animal sperm (Lin et al., 2006; reviewed in Culotta and Daly, 2013). Thus, an appealing hypothesis, which deserves future investigations, is that like its yeast ortholog, NRAMP2, could build up a pool of cytosolic antioxidant Mn in Arabidopsis.

NRAMP2 Is Crucial for Mn Nutrition upon Mn Limitation

Within the cell, the TGN is a sorting hub for post-Golgi trafficking pathways involved in secretory or vacuolar transport. The presence of NRAMP2 in the TGN suggests it plays a role in the mobilization of Mn from, or into, these vesicles. Since proteins of the NRAMP family use the proton gradient as a driving force (Nevo and Nelson, 2006), they are known to transport metals from a more acidic to a less acidic compartment. Consequently, except for the few studies that proposed that transport by NRAMP occurs in the direction of the exit of metals from the cytosol (Techau et al., 2007; García-Rodríguez et al., 2015), the vast majority of the reported NRAMP transporters, including all plant members, import metals into the cytosol (Cailliatte et al., 2010). Following the proton co-transport dogma, the presence of NRAMP2 on TGN vesicles, which are more acidic than the cytosol (Martinière et al., 2013), is consistent with NRAMP2 mediating Mn influx into the cytosol. In addition, the failure of NRAMP2 to rescue the *pmr1*Δ yeast mutant defective in Golgi Mn uptake also argues against an activity of NRAMP2 in transport toward the TGN lumen. Several observations support the hypothesis that NRAMP2 releases Mn from the TGN into the cytosol and hence contributes to the buildup of a cytosolic Mn pool that would be used to feed Mn both to downstream organelles and to the antioxidant machinery of the cell: (1) The Mn content in two organelles, vacuoles and chloroplasts, correlates with the expression level of NRAMP2; vacuoles and chloroplasts of the *nramp2* mutant both harbor low Mn content; (2) in yeast, NRAMP2 expression rescues the mitochondrial *mtm1*Δ mutant, the growth of which depends on high Mn supply to the mitochondria (Yang et al., 2006); these two arguments strongly support a role for NRAMP2 in fueling the cytosolic Mn pool, which serves as a source of Mn to the main organelles; (3) NRAMP2 is also able to functionally compensate for the absence of cytosolic Sod1p in yeast, which we propose may occur through the accumulation of cytosolic Mn antioxidant species having SOD activity. If a similar alternate SOD system relying on Mn antioxidant species in the cytosol exists in plants, NRAMP2 represents a reasonable candidate to supply these from vesicular compartments.

Based on the phenotypes of an *nramp2* knockdown allele and its combination with the *nramp3* and *nramp4* mutations, we propose a model in which under Mn-limiting conditions, a pool of Mn stored in the TGN is released by NRAMP2 and carried by a yet to be identified pathway to the vacuole, from which it is secreted by NRAMP3 and NRAMP4 to provide a significant portion of the Mn ions that reach the chloroplasts (Figure 10). In-depth analysis of the cellular function of candidate Mn transporters, including members of the ECA, MTP, and NRAMP families, should identify additional important actors and shed further light into the Mn trafficking pathway in plant cells, although chemical or genetically encoded Mn sensors will be needed to image Mn movement between cell compartments.

METHODS

Plant Materials and Growth Conditions

Two *Arabidopsis thaliana NRAMP2* mutant lines were used: *nramp2-3* (unreferenced SALK line kindly provided by Jose Alonso) and *nramp2-4* (GK-306A04), both containing a T-DNA inserted in the 5′-untranslated region of the *NRAMP2* gene, at 68 and 43 bp upstream of the ATG start codon, respectively. The *nramp1-1* mutant was described previously (Cailliatte et al., 2010). The *nramp3-2 nramp4-2* double mutant was generated by crossing SALK line 023049 (*nramp3-2*) with SALK line 003737 (*nramp4-2*).

Arabidopsis seedlings (ecotype Columbia-0) were grown in vitro under sterile conditions at 21°C with an 8-h-light (composed of 50% sodium-vapor lamps and 50% metal halide [HQI] lamps)/16-h-dark cycle. Seeds were surface sterilized and sown on half-strength Murashige and Skoog medium containing 1% sucrose, 2.5 mM MES, and either 0.6% agar for horizontal cultures or 1% agar for vertical cultures. The pH was adjusted to 5.7 with KOH.

For the hydroponic growth experiments, seeds were sown on vertical plates. Eight-day-old seedlings were placed in a modified Hoagland solution containing 0.25 mM NH_4NO_3, 1 mM $Ca(NO_3)_2$, 0.2 mM KH_2PO_4, 1.4 mM KNO_3, 0.4 mM $MgSO_4$, 20 μM Fe(III)-Na-EDTA, 4.5 μM H_3BO_3, 0.03 μM $CuSO_4$, 0.07 μM $ZnSO_4$, and 0.02 mM MoO_3. For control

conditions, the medium was supplemented with 5 μM $MnSO_4$. The nutrient solution was renewed weekly. The hydroponic cultures were grown in a controlled environment (8-h-light 23°C/16-h-dark cycles, 20°C, 200 $\mu E \cdot s^{-1}$ light intensity, 70% relative humidity) for the amount of time indicated in the figure legends.

Plasmid Constructs

For tissue-specific expression studies, 983 bp of the promoter region located upstream of the *NRAMP2* initiation codon were amplified by PCR from BAC F8G22 using forward primers OCC53 and OCC54 (see list of primers in Supplemental Table 6), introducing an *Xba*I and *Nco*I site, respectively. The PCR product was cloned into the pBKS+-GUS vector. The *ProNRAMP2:GUS* fusion cassette was then transferred into the *Xba*I site of the pGreen29 binary vector. For the *ProUB10:NRAMP2-GFP* fusion construct, the NRAMP2 cDNA was amplified without its stop codon using primers NR2_ORF-F and NR2_ORF-R and cloned into the pDONR 207 entry vector (Gateway; Invitrogen). The *NRAMP2* ORF was then subcloned into the pUBC-GFP-Dest vector (Grefen et al., 2010) to generate a C-terminal GFP fusion. The GV3101 strain of *Agrobacterium tumefaciens* containing the *ProNRAMP2:GUS* and *ProUB10:NRAMP2-GFP* constructs were transformed into Arabidopsis ecotype Col-0 wild-type and *nramp2-3*, respectively, by the floral dip method (Clough and Bent, 1998).

Cell Fractionation

Chloroplasts Isolation

Protoplasts were isolated by enzymatic digestion of ~3 g of leaves cut in 1- to 2-mm-wide stripes in 10 mL of MCP buffer (500 mM sorbitol, 1 mM $CaCl_2$, and 20 mM MES, adjusted to pH 6.0 with KOH) supplemented with 0.4% (w/v) Macerozyme R10 (Duchefa Biochemie) and 0.8% (w/v) Cellulase Onozuka R10 (Duchefa Biochemie) at 30°C for 1 h 30 min. The protoplasts were filtered through a 75-mm nylon mesh, pelleted (200*g*, 5 min, 4°C), and washed twice with MCP buffer. The protoplasts were diluted to 2×10^6 cells mL^{-1} and lysed by filtration through a polyester mesh (Spectrum; pore size 21 μm). The lysed protoplasts were kept on ice. Percoll step gradient was as follows: bottom phase, 1 volume of 85% Percoll in washing medium (300 mM sorbitol, 40 mM Tricine, pH 7.6, 2.5 mM EDTA, and 0.5 mM $MgCl_2$); top phase, 1 volume of 40% Percoll in washing medium. Chloroplasts were isolated by loading the protoplast lysate on top of the Percoll step gradient followed by centrifugation (2500*g*, 10 min, 4°C, without brake) in a swinging rotor. Intact chloroplasts were recovered by centrifugation at 200*g* for 5 min at 4°C (with no brake) from the 40/85% Percoll interphase and washed two times with cold washing medium. The integrity of the chloroplasts was verified by microscopy, and the number of chloroplasts was estimated by counting with a Neubauer chamber.

Vacuole Isolation

The vacuole isolation was performed as previously described (Lanquar et al., 2010) with some modifications. Briefly, the protoplasts were lysed by the addition of an equal volume of protoplast lysis buffer (200 mM sorbitol, 10% [w/v] Ficoll 400, 20 mM EDTA, 10 mM HEPES-KOH, pH 8, 0.15% [w/v] BSA, and 2 mM DTT, and 5 μg/mL neutral red) prewarmed at 37°C. Protoplast lysis was monitored microscopically, and lysed protoplasts were kept on ice. Vacuoles were isolated using a step gradient in swinging rotors (1500*g*, 20 min, 4C): bottom phase, 1 volume of lysed protoplasts; middle phase, 0.8 volume of lysis buffer diluted in vacuole buffer to a final concentration of 4% (w/v) Ficoll; top phase, 0.2 volume of vacuole buffer (500 mM sorbitol, 10 mM HEPES, pH 7.5 [KOH], 0.15% [w/v] BSA, and 4 mM DTT). Vacuoles were recovered as a thin red layer at the interface between the middle phase and the top phase. The purity of the vacuole preparation was monitored by microscopy and the number of vacuoles was estimated by counting with a Neubauer chamber.

Gene Expression Analysis

Total RNA was extracted using the Trizol reagent (Invitrogen) following the manufacturer's instructions. Reverse transcription was performed with oligo(dT) primers on 1 to 2 μg of total RNA digested with DNase I (Thermo Scientific) using a RevertAid first-strand cDNA synthesis kit (Thermo Scientific) according to the manufacturer's protocols. The qPCRs were performed on the Roche Light Cycler 480 II instrument using the primer sets listed in Supplemental Table 6 and SYBR Premix Ex Taq (Tli RNaseH Plus Bulk; Takara).

GUS Histochemical Analysis

Samples were vacuum infiltrated for 20 min and incubated for 18 h in GUS buffer containing 50 mM $NaPO_4$, pH 7.4, 2 mM ferrocyanide, 2 mM ferricyanide, 0.05% Triton X-100, and 1 mM X-Gluc (5-bromo-4-chloro-3-indolyl-β-D-glucuronide). The samples were then soaked in phosphate buffer (50 mM $NaPO_4$, pH 7.2) and prefixed for 3 h in phosphate buffer containing 2% paraformaldehyde and 0.5% glutaraldehyde. The samples were cleared with successive washes of increasing ethanol concentrations from 50 to 100% for direct observation or embedded in 2-hydroxyethyl methacrylate (Technovit 7100; Heraus-Kulzer). Thin cross sections (5 μm) were cut using a Leica RM 2165 microtome, counterstained with Schiff dye, and observed under an Olympus BH2 microscope.

Yeast Strains and Growth Conditions

Yeast cells were grown at 30°C in YPD medium (2% glucose, 2% tryptone, and 1% yeast extract) or SD medium (2% glucose, 0,7% yeast nitrogen base with ammonium sulfate, and 50 mM succinic acid, pH5.5). Wild-type BY4741 (*MATa; his3, leu2, met15, ura3*), *smf1Δ* (*MATa; his3, leu2, met15, ura3, smf1::kanMX4*), *smf2Δ* (*MATa; his3, leu2, met15, ura3, smf2::kanMX4*), *mtm1Δ* (*MATa; his3, leu2, met15, ura3, mtm1::kanMX4*), *pmr1Δ* (*MATa; his3, leu2, met15, ura3, pmr1::kanMX4*), and *sod1*Δ (*MATa his3::1 leu2::0 met15::0 ura3::0 sod1::kanMX4*) cells were transformed with pYPGE15-*NRAMP2* (Curie et al., 2000), where NRAMP2 is expressed under the control of the constitutive high yeast phosphoglycerate kinase promoter or pYPGE15 empty vector using electroporation. Yeast transformants were selected on medium lacking uracil.

For growth tests, yeast cells were first grown in liquid culture overnight at 30°C in SD medium. The cultures were adjusted to $OD_{600} = 0.3$, and aliquots of 5-fold serial dilutions were plated on 2% (w/v) agar plates containing SD-Ura medium supplemented with EGTA or $MnSO_4$. In the case of EGTA plates, SD medium was prepared with 0.7% YNB with low metal concentration (US Biological). To monitor the steady state manganese levels in yeast cells, the strains were grown in 20 mL SD-Ura medium to an OD_{600} = 1.5, pelleted, and washed three times with 10 mM EDTA and twice with deionized water.

Superoxide Dismutase Activity

In Yeast

Yeast cells were propagated in YPD medium to an OD_{600} of 1.5, harvested, and washed with cold water before being broken by agitation in the presence of glass beads in extraction buffer (100 mM $NaPO_4$, pH 7.8, 50 mM NaCl, 5 mM EDTA, 5 mM EGTA, 0.1% Triton X-100, 100 μg/mL phenylmethylsulfonyl fluoride, 1 μg/mL pepstatin A, and 1 μg/mL

leupeptin). The homogenate was centrifuged for 5 min at 2500*g* and the protein pellet was solubilized in extraction buffer.

In Plants

Leaves were ground in liquid nitrogen and resuspended in cold extraction buffer (40 mM K_2HPO_4, 10 mM KH_2PO_4, 6 mM ascorbic acid, 0.05% β-mercaptoethanol, and 0.2% Triton X-100) for 2 min, followed by 10 min centrifugation at 14,000 rpm at 4°C.

Proteins were loaded onto a 12% nondenaturing PAGE gel and the SOD activity was measured by NBT staining. Briefly, the gel was soaked in NBT solution (1 mg/mL) for 20 min in the dark and transferred into staining solution (33 mM K_2HPO_4, 3.3 mM KH_2PO_4, 1 mg/mL riboflavin, and 0.3% TEMED) for 20 min in the dark. The gel was rinsed in distilled water before being exposed to high light until the bands appeared.

Manganese Content Measurements

The roots were washed for 10 min with 10 mM EDTA and 5 min with 30 mM $MgCl_2$, followed by two rinses in deionized water. Shoots were simply rinsed twice with deionized water. Plant samples and yeast pellets were dried at 80°C for 4 d. For mineralization, the tissues were digested completely in 50% HNO3 and 7.5% H_2O_2 using the Speedwave 2 microwave digestion system (Berghof). Mn measurements were performed by atomic emission spectrometry (4200 MP-AES; Agilent).

Photosynthesis Fluorescence Measurements

A kinetic imaging fluorometer (FluorCam FC 800-O; Photon Systems Instruments) was used to capture fluorescence images and to estimate the maximal photochemical efficiency of PSII [$F_v/F_m = (F_m - F_o)/F_m$] and effective photochemical efficiency of PSII (ΦPSII) parameters. Control and Mn-free Arabidopsis plants were dark-adapted (30 min), and all fluorescence measurements were performed in vivo at room temperature. Saturating flashes (1000 $\mu mol \cdot m^{-2} \cdot s^{-1)}$ were used to measure the maximum fluorescence.

Chlorophyll Measurements

A SPAD meter (SPAD-502Plus; Konica-Minolta) was used to take SPAD values from two fully expanded young leaves on each plant. A total of six plants were measured for each genotype and growth condition, and three SPAD values per leaf were averaged as the mean SPAD value of the leaf.

Detection of Superoxide Radicals

O_2^- ions were visualized by staining leaves (leaf nos. 8–10) with NBT. Briefly, excised leaves were vacuum infiltrated in NBT staining solution (1 mg/mL NBT and 10 mM Na_2HPO_4) for 20 min and incubated for 2 to 3 h under light. Chlorophyll was removed by incubating the leaves for 5 min in boiling 96% ethanol. After cooling, the leaves were immersed in water and photographed in 10% glycerol.

Permeability Test with TB

Excised leaves were submerged into an aqueous solution of filtered 0.05% (w/v) TB in a small Petri dish for the indicated amount of time. The leaves were gently washed with water to remove excess TB.

Cutin Load Analysis

Three to five fully developed leaves were used per replicate. Freshly collected leaves were scanned to measure their surfaces and immediately incubated in hot isopropanol for 30 min at 85°C. After cooling, the solvent was eliminated and the leaves were extensively delipidated by extracting the soluble lipids successively with $CHCl_3$:CH_3OH (2:1, v/v), $CHCl_3$:CH_3OH (1:1, v/v), $CHCl_3$:CH_3OH (1:2, v/v), and CH_3OH. Each delipidation step was performed for 24 h at room temperature on a rotating wheel at 40 rpm. The delipidated leaves were dried in a fume hood at room temperature for 2 d and then in a desiccator for another 2 d. Cutin analysis was then performed as described previously (Domergue et al., 2010).

Confocal Microscopy Analysis

Nicotiana tabacum leaves were agroinfiltrated with the recombinant Agrobacterium strains (strain GV3101, infiltration solution OD_{600} = 0.1). After 2 d, confocal imaging was performed using a Leica TCS SP8 laser scanning microscope with a 63× oil N.A. 1.4 immersion objective. Emission fluorescence of CFP, GFP, and mCherry was collected in line sequential scanning mode at 458, 488, and 561 nm excitation, respectively. The emitted signal was collected between 462 and 485 nm, 500 and 535 nm, and 580 and 630 nm for CFP, GFP, and mCherry/RFP, respectively, and images were acquired with the best lateral and axial resolution (pixel size 60/70 nm). Images were processed using ImageJ software. For the FM4-64 endocytosis experiments, roots of 7-d-old Arabidopsis seedlings were incubated for 5 min in 10 μM FM4-64 and rinsed with water at the time indicated in the figure legends. The set of cell compartment markers (plasmids or Arabidopsis lines) used was as follows: Px-rk983-mCherry (Nelson et al., 2002), Arabidopsis Wave lines (Geldner et al., 2009), ERD2-CFP (Brandizzi et al., 2002), and SYP61-mRFP (Foresti et al., 2010).

Colocalization coefficients were computed with the JACoP plug-in ($r_{pearson}$, Pearson correlation coefficient; M1 and M2, Mander's overlap coefficients above threshold) (Bolte and Cordelières, 2006). In each experiment, 7 to 10 cells from the root elongation zone were analyzed individually for each genotype.

Accession Numbers

Sequence data from this article can be found in the Arabidopsis Genome Initiative or GenBank/EMBL databases under accession numbers At1g80830 (NRAMP1), At1g47240 (NRAMP2), At2g23150 (NRAMP3), At5g67330 (NRAMP4), and At3g18780 (ACT2).

Supplemental Data

Supplemental Figure 1. *nramp2* mutant alleles are chlorotic under Mn deficiency.

Supplemental Figure 2. Expression of *NRAMP1* is not modified in the *nramp2-3* mutant.

Supplemental Figure 3. Confocal microscopy observations of NRAMP2-GFP fluorescence and colocalization with markers of various cell compartments.

Supplemental Figure 4. *nramp2-3*, but not the Mn-deficient mutant *nramp1-1*, shows leaf permeability defects.

Supplemental Figure 5. Production of superoxide ions in the *nramp2 nramp3 nramp4* triple mutant.

Supplemental Table 1. Mn concentration ($\mu g \cdot g^{-1}$ DW) in rosette leaves and roots of wild-type, *nramp2-3*, and the *OxNR2* #3- and *OxNR2* #6-complemented lines.

Supplemental Table 2. Quantitative analysis of NRAMP2-GFP colocalization with Golgi markers.

Supplemental Table 3. Photosynthetic activity of *nramp2* mutant alleles and the complemented line OxNR2 #3.

Supplemental Table 4. Mn content is altered in vacuoles and chloroplasts of the *nramp2-3* mutant.

Supplemental Table 5. Photosynthetic activity of single *nramp2-3*, double *nramp3-2 nramp4-2*, and triple *nramp2-3 nramp3-2 nramp4-2* mutants.

Supplemental Table 6. List of the gene-specific primers used.

Supplemental File 1. ANOVA table.

ACKNOWLEDGMENTS

This work was funded by the Agence Nationale pour la Recherche through ANR Grants PLANTMAN (ANR-2011-BSV6-004) and MANOMICS (ANR-2011-ISV6-001-01), by the Centre National de la Recherche Scientifique, and by the Institut National de la Recherche Agronomique. Microscopy observations were made at the Montpellier RIO Imaging facility (http://www.mri.cnrs.fr/). We thank Jose Alonso for providing *nramp2-3* seeds. We also thank Sandrine Chay and Brigitte Touraine for assistance with MP-AES and FluorCam measurements, respectively. S.M. and L.C. were supported by the Agence Nationale pour la Recherche, and R.C. was supported by the French Ministry of Agriculture and Fisheries.

AUTHOR CONTRIBUTIONS

S.A., R.C., S.M., and C.C. designed the research. S.A., R.C., C.A., L.D., D.C., L.C., and F.D. performed research and analyzed data. C.A. performed confocal imaging experiments and statistical analysis of colocalizations. F.D. performed lipid analyses. J.-F.B. contributed to discussions and constructive comments on the manuscript. S.A. and C.C. wrote the manuscript.

Received July 24, 2017; revised November 17, 2017; accepted November 25, 2017; published November 27, 2017.

REFERENCES

Agorio, A., Giraudat, J., Bianchi, M.W., Marion, J., Espagne, C., Castaings, L., Lelièvre, F., Curie, C., Thomine, S., and Merlot, S. (2017). Phosphatidylinositol 3-phosphate-binding protein AtPH1 controls the localization of the metal transporter NRAMP1 in Arabidopsis. Proc. Natl. Acad. Sci. USA **114:** E3354–E3363.

Allen, M.D., Kropat, J., Tottey, S., Del Campo, J.A., and Merchant, S.S. (2007). Manganese deficiency in Chlamydomonas results in loss of photosystem II and MnSOD function, sensitivity to peroxides, and secondary phosphorus and iron deficiency. Plant Physiol. **143:** 263–277.

Barberon, M., Vermeer, J.E., De Bellis, D., Wang, P., Naseer, S., Andersen, T.G., Humbel, B.M., Nawrath, C., Takano, J., Salt, D.E., and Geldner, N. (2016). Adaptation of root function by nutrient-induced plasticity of endodermal differentiation. Cell **164:** 447–459.

Bolte, S., and Cordelières, F.P. (2006). A guided tour into subcellular colocalization analysis in light microscopy. J. Microsc. **224:** 213–232.

Brandizzi, F., Frangne, N., Marc-Martin, S., Hawes, C., Neuhaus, J.M., and Paris, N. (2002). The destination for single-pass membrane proteins is influenced markedly by the length of the hydrophobic domain. Plant Cell **14:** 1077–1092.

Cailliatte, R., Lapeyre, B., Briat, J.F., Mari, S., and Curie, C. (2009). The NRAMP6 metal transporter contributes to cadmium toxicity. Biochem. J. **422:** 217–228.

Cailliatte, R., Schikora, A., Briat, J.F., Mari, S., and Curie, C. (2010). High-affinity manganese uptake by the metal transporter NRAMP1 is essential for Arabidopsis growth in low manganese conditions. Plant Cell **22:** 904–917.

Castaings, L., Caquot, A., Loubet, S., and Curie, C. (2016). The high-affinity metal transporters NRAMP1 and IRT1 team up to take up iron under sufficient metal provision. Sci. Rep. **6:** 37222.

Clough, S.J., and Bent, A.F. (1998). Floral dip: a simplified method for Agrobacterium-mediated transformation of *Arabidopsis thaliana*. Plant J. **16:** 735–743.

Cohen, A., Nelson, H., and Nelson, N. (2000). The family of SMF metal ion transporters in yeast cells. J. Biol. Chem. **275:** 33388–33394.

Culotta, V.C., and Daly, M.J. (2013). Manganese complexes: diverse metabolic routes to oxidative stress resistance in prokaryotes and yeast. Antioxid. Redox Signal. **19:** 933–944.

Curie, C., Alonso, J.M., Le Jean, M., Ecker, J.R., and Briat, J.F. (2000). Involvement of NRAMP1 from *Arabidopsis thaliana* in iron transport. Biochem. J. **347:** 749–755.

Delhaize, E., Gruber, B.D., Pittman, J.K., White, R.G., Leung, H., Miao, Y., Jiang, L., Ryan, P.R., and Richardson, A.E. (2007). A role for the AtMTP11 gene of Arabidopsis in manganese transport and tolerance. Plant J. **51:** 198–210.

del Río, L.A., Sandalio, L.M., Altomare, D.A., and Zilinskas, B.A. (2003). Mitochondrial and peroxisomal manganese superoxide dismutase: differential expression during leaf senescence. J. Exp. Bot. **54:** 923–933.

Dinneny, J.R., Long, T.A., Wang, J.Y., Jung, J.W., Mace, D., Pointer, S., Barron, C., Brady, S.M., Schiefelbein, J., and Benfey, P.N. (2008). Cell identity mediates the response of Arabidopsis roots to abiotic stress. Science **320:** 942–945.

Divol, F., Couch, D., Conéjéro, G., Roschzttardtz, H., Mari, S., and Curie, C. (2013). The Arabidopsis YELLOW STRIPE LIKE4 and 6 transporters control iron release from the chloroplast. Plant Cell **25:** 1040–1055.

Domergue, F., Vishwanath, S.J., Joubès, J., Ono, J., Lee, J.A., Bourdon, M., Alhattab, R., Lowe, C., Pascal, S., Lessire, R., and Rowland, O. (2010). Three Arabidopsis fatty acyl-coenzyme A reductases, FAR1, FAR4, and FAR5, generate primary fatty alcohols associated with suberin deposition. Plant Physiol. **153:** 1539–1554.

Drakakaki, G., van de Ven, W., Pan, S., Miao, Y., Wang, J., Keinath, N.F., Weatherly, B., Jiang, L., Schumacher, K., Hicks, G., and Raikhel, N. (2012). Isolation and proteomic analysis of the SYP61 compartment reveal its role in exocytic trafficking in Arabidopsis. Cell Res. **22:** 413–424.

Eroglu, S., Meier, B., von Wirén, N., and Peiter, E. (2016). The vacuolar manganese transporter MTP8 determines tolerance to iron deficiency-induced chlorosis in arabidopsis. Plant Physiol. **170:** 1030–1045.

Foresti, O., Gershlick, D.C., Bottanelli, F., Hummel, E., Hawes, C., and Denecke, J. (2010). A recycling-defective vacuolar sorting receptor reveals an intermediate compartment situated between prevacuoles and vacuoles in tobacco. Plant Cell **22:** 3992–4008.

García-Rodríguez, N., Díaz de la Loza, Mdel.C., Andreson, B., Monje-Casas, F., Rothstein, R., and Wellinger, R.E. (2012). Impaired manganese metabolism causes mitotic misregulation. J. Biol. Chem. **287:** 18717–18729.

García-Rodríguez, N., Manzano-López, J., Muñoz-Bravo, M., Fernández-García, E., Muñiz, M., and Wellinger, R.E. (2015). Manganese redistribution by calcium-stimulated vesicle trafficking bypasses the need for P-type ATPase function. J. Biol. Chem. **290:** 9335–9347.

Geldner, N., Dénervaud-Tendon, V., Hyman, D.L., Mayer, U., Stierhof, Y.D., and Chory, J. (2009). Rapid, combinatorial analysis of

membrane compartments in intact plants with a multicolor marker set. Plant J. **59:** 169–178.

Grefen, C., Donald, N., Hashimoto, K., Kudla, J., Schumacher, K., and Blatt, M.R. (2010). A ubiquitin-10 promoter-based vector set for fluorescent protein tagging facilitates temporal stability and native protein distribution in transient and stable expression studies. Plant J. **64:** 355–365.

Hebbern, C.A., Laursen, K.H., Ladegaard, A.H., Schmidt, S.B., Pedas, P., Bruhn, D., Schjoerring, J.K., Wulfsohn, D., and Husted, S. (2009). Latent manganese deficiency increases transpiration in barley (*Hordeum vulgare*). Physiol. Plant. **135:** 307–316.

Hoffmann-Benning, S., and Kende, H. (1994). Cuticle biosynthesis in rapidly growing internodes of deepwater rice. Plant Physiol. **104:** 719–723.

Ishimaru, Y., Takahashi, R., Bashir, K., Shimo, H., Senoura, T., Sugimoto, K., Ono, K., Yano, M., Ishikawa, S., Arao, T., Nakanishi, H., and Nishizawa, N.K. (2012). Characterizing the role of rice NRAMP5 in manganese, iron and cadmium transport. Sci. Rep. **2:** 286.

Kim, S.A., Punshon, T., Lanzirotti, A., Li, L., Alonso, J.M., Ecker, J.R., Kaplan, J., and Guerinot, M.L. (2006). Localization of iron in Arabidopsis seed requires the vacuolar membrane transporter VIT1. Science **314:** 1295–1298.

Lanquar, V., Ramos, M.S., Lelièvre, F., Barbier-Brygoo, H., Krieger-Liszkay, A., Krämer, U., and Thomine, S. (2010). Export of vacuolar manganese by AtNRAMP3 and AtNRAMP4 is required for optimal photosynthesis and growth under manganese deficiency. Plant Physiol. **152:** 1986–1999.

Lanquar, V., Lelièvre, F., Bolte, S., Hamès, C., Alcon, C., Neumann, D., Vansuyt, G., Curie, C., Schröder, A., Krämer, U., Barbier-Brygoo, H., and Thomine, S. (2005). Mobilization of vacuolar iron by AtNRAMP3 and AtNRAMP4 is essential for seed germination on low iron. EMBO J. **24:** 4041–4051.

Lin, Y.T., Hoang, H., Hsieh, S.I., Rangel, N., Foster, A.L., Sampayo, J.N., Lithgow, G.J., and Srinivasan, C. (2006). Manganous ion supplementation accelerates wild type development, enhances stress resistance, and rescues the life span of a short-lived *Caenorhabditis elegans* mutant. Free Radic. Biol. Med. **40:** 1185–1193.

Luk, E., Carroll, M., Baker, M., and Culotta, V.C. (2003). Manganese activation of superoxide dismutase 2 in *Saccharomyces cerevisiae* requires MTM1, a member of the mitochondrial carrier family. Proc. Natl. Acad. Sci. USA **100:** 10353–10357.

Luk, E.E., and Culotta, V.C. (2001). Manganese superoxide dismutase in *Saccharomyces cerevisiae* acquires its metal co-factor through a pathway involving the Nramp metal transporter, Smf2p. J. Biol. Chem. **276:** 47556–47562.

Marschner, H., Romheld, V., and Kissel, M. (1986). Different strategies in higher plants in mobilization and uptake of iron. J. Plant Nutr. **9:** 3–7.

Martinière, A., Bassil, E., Jublanc, E., Alcon, C., Reguera, M., Sentenac, H., Blumwald, E., and Paris, N. (2013). In vivo intracellular pH measurements in tobacco and Arabidopsis reveal an unexpected pH gradient in the endomembrane system. Plant Cell **25:** 4028–4043.

McNaughton, R.L., Reddi, A.R., Clement, M.H., Sharma, A., Barnese, K., Rosenfeld, L., Gralla, E.B., Valentine, J.S., Culotta, V.C., and Hoffman, B.M. (2010). Probing in vivo Mn^{2+} speciation and oxidative stress resistance in yeast cells with electron-nuclear double resonance spectroscopy. Proc. Natl. Acad. Sci. USA **107:** 15335–15339.

Mills, R.F., Doherty, M.L., López-Marqués, R.L., Weimar, T., Dupree, P., Palmgren, M.G., Pittman, J.K., and Williams, L.E. (2008). ECA3, a Golgi-localized P2A-type ATPase, plays a crucial role in manganese nutrition in Arabidopsis. Plant Physiol. **146:** 116–128.

Milner, M.J., Seamon, J., Craft, E., and Kochian, L.V. (2013). Transport properties of members of the ZIP family in plants and their role in Zn and Mn homeostasis. J. Exp. Bot. **64:** 369–381.

Momonoi, K., Yoshida, K., Mano, S., Takahashi, H., Nakamori, C., Shoji, K., Nitta, A., and Nishimura, M. (2009). A vacuolar iron transporter in tulip, TgVit1, is responsible for blue coloration in petal cells through iron accumulation. Plant J. **59:** 437–447.

Nelson, N., Sacher, A., and Nelson, H. (2002). The significance of molecular slips in transport systems. Nat. Rev. Mol. Cell Biol. **3:** 876–881.

Nevo, Y., and Nelson, N. (2006). The NRAMP family of metal-ion transporters. Biochim. Biophys. Acta **1763:** 609–620.

Nickelsen, J., and Rengstl, B. (2013). Photosystem II assembly: from cyanobacteria to plants. Annu. Rev. Plant Biol. **64:** 609–635.

Pedas, P., Schiller Stokholm, M., Hegelund, J.N., Ladegård, A.H., Schjoerring, J.K., and Husted, S. (2014). Golgi localized barley MTP8 proteins facilitate Mn transport. PLoS One **9:** e113759.

Peiter, E., Montanini, B., Gobert, A., Pedas, P., Husted, S., Maathuis, F.J., Blaudez, D., Chalot, M., and Sanders, D. (2007). A secretory pathway-localized cation diffusion facilitator confers plant manganese tolerance. Proc. Natl. Acad. Sci. USA **104:** 8532–8537.

Pittman, J.K., Shigaki, T., Marshall, J.L., Morris, J.L., Cheng, N.H., and Hirschi, K.D. (2004). Functional and regulatory analysis of the *Arabidopsis thaliana* CAX2 cation transporter. Plant Mol. Biol. **56:** 959–971.

Portnoy, M.E., Liu, X.F., and Culotta, V.C. (2000). *Saccharomyces cerevisiae* expresses three functionally distinct homologues of the nramp family of metal transporters. Mol. Cell. Biol. **20:** 7893–7902.

Ravet, K., Touraine, B., Kim, S.A., Cellier, F., Thomine, S., Guerinot, M.L., Briat, J.F., and Gaymard, F. (2009). Post-translational regulation of AtFER2 ferritin in response to intracellular iron trafficking during fruit development in Arabidopsis. Mol. Plant **2:** 1095–1106.

Roth, J.A. (2006). Homeostatic and toxic mechanisms regulating manganese uptake, retention, and elimination. Biol. Res. **39:** 45–57.

Rudolph, H.K., Antebi, A., Fink, G.R., Buckley, C.M., Dorman, T.E., LeVitre, J., Davidow, L.S., Mao, J.I., and Moir, D.T. (1989). The yeast secretory pathway is perturbed by mutations in PMR1, a member of a Ca^{2+} ATPase family. Cell **58:** 133–145.

Sasaki, A., Yamaji, N., Yokosho, K., and Ma, J.F. (2012). Nramp5 is a major transporter responsible for manganese and cadmium uptake in rice. Plant Cell **24:** 2155–2167.

Schmidt, S.B., Jensen, P.E., and Husted, S. (2016). Manganese deficiency in plants: the impact on photosystem II. Trends Plant Sci. **21:** 622–632.

Schneider, A., et al. (2016). The evolutionarily conserved protein PHOTOSYNTHESIS AFFECTED MUTANT71 is required for efficient manganese uptake at the thylakoid membrane in Arabidopsis. Plant Cell **28:** 892–910.

Su, Z., Chai, M.F., Lu, P.L., An, R., Chen, J., and Wang, X.C. (2007). AtMTM1, a novel mitochondrial protein, may be involved in activation of the manganese-containing superoxide dismutase in Arabidopsis. Planta **226:** 1031–1039.

Supek, F., Supekova, L., Nelson, H., and Nelson, N. (1996). A yeast manganese transporter related to the macrophage protein involved in conferring resistance to mycobacteria. Proc. Natl. Acad. Sci. USA **93:** 5105–5110.

Tanaka, T., Tanaka, H., Machida, C., Watanabe, M., and Machida, Y. (2004). A new method for rapid visualization of defects in leaf

cuticle reveals five intrinsic patterns of surface defects in Arabidopsis. Plant J. **37:** 139–146.

Techau, M.E., Valdez-Taubas, J., Popoff, J.F., Francis, R., Seaman, M., and Blackwell, J.M. (2007). Evolution of differences in transport function in Slc11a family members. J. Biol. Chem. **282:** 35646–35656.

Thomine, S., Wang, R., Ward, J.M., Crawford, N.M., and Schroeder, J.I. (2000). Cadmium and iron transport by members of a plant metal transporter family in Arabidopsis with homology to Nramp genes. Proc. Natl. Acad. Sci. USA **97:** 4991–4996.

Uemura, T., and Nakano, A. (2013). Plant TGNs: dynamics and physiological functions. Histochem. Cell Biol. **140:** 341–345.

Whittaker, M.M., Penmatsa, A., and Whittaker, J.W. (2015). The Mtm1p carrier and pyridoxal 5′-phosphate cofactor trafficking in yeast mitochondria. Arch. Biochem. Biophys. **568:** 64–70.

Wilson, D.O., Boswell, F.C., Ohki, K., Parker, M.B., Shuman, L.M., and Jellum, M.D. (1982). Changes in soybean seed oil and protein as influenzed by manganese nutrition. Crop Sci. **22:** 948–952.

Wu, Z., Liang, F., Hong, B., Young, J.C., Sussman, M.R., Harper, J.F., and Sze, H. (2002). An endoplasmic reticulum-bound Ca^{2+}/Mn^{2+} pump, ECA1, supports plant growth and confers tolerance to Mn^{2+} stress. Plant Physiol. **130:** 128–137.

Yang, M., Cobine, P.A., Molik, S., Naranuntarat, A., Lill, R., Winge, D.R., and Culotta, V.C. (2006). The effects of mitochondrial iron homeostasis on cofactor specificity of superoxide dismutase 2. EMBO J. **25:** 1775–1783.

Yeats, T.H., and Rose, J.K. (2013). The formation and function of plant cuticles. Plant Physiol. **163:** 5–20.

Zhang, Y., Xu, Y.H., Yi, H.Y., and Gong, J.M. (2012). Vacuolar membrane transporters OsVIT1 and OsVIT2 modulate iron translocation between flag leaves and seeds in rice. Plant J. **72:** 400–410.

NOTE ADDED IN PROOF

While this manuscript was under revision, two mutant alleles of *NRAMP2* (*nramp2*-1 and *nramp2*-2) were reported.

Gao, H., Xie, W., Yang, C., Xu, J., Li, J., Wang, H., Chen, X., and Huang, C.F. (2017) NRAMP2, a trans-Golgi network-localized manganese transporter, is required for Arabidopsis root growth under manganese deficiency. New Phytol. **217:** 179–193.